iScience

CellPress
OPEN ACCESS

Article

Non-canonical function of DPP4 promotes cognitive impairment through ERp29-associated mitochondrial calcium overload in diabetes

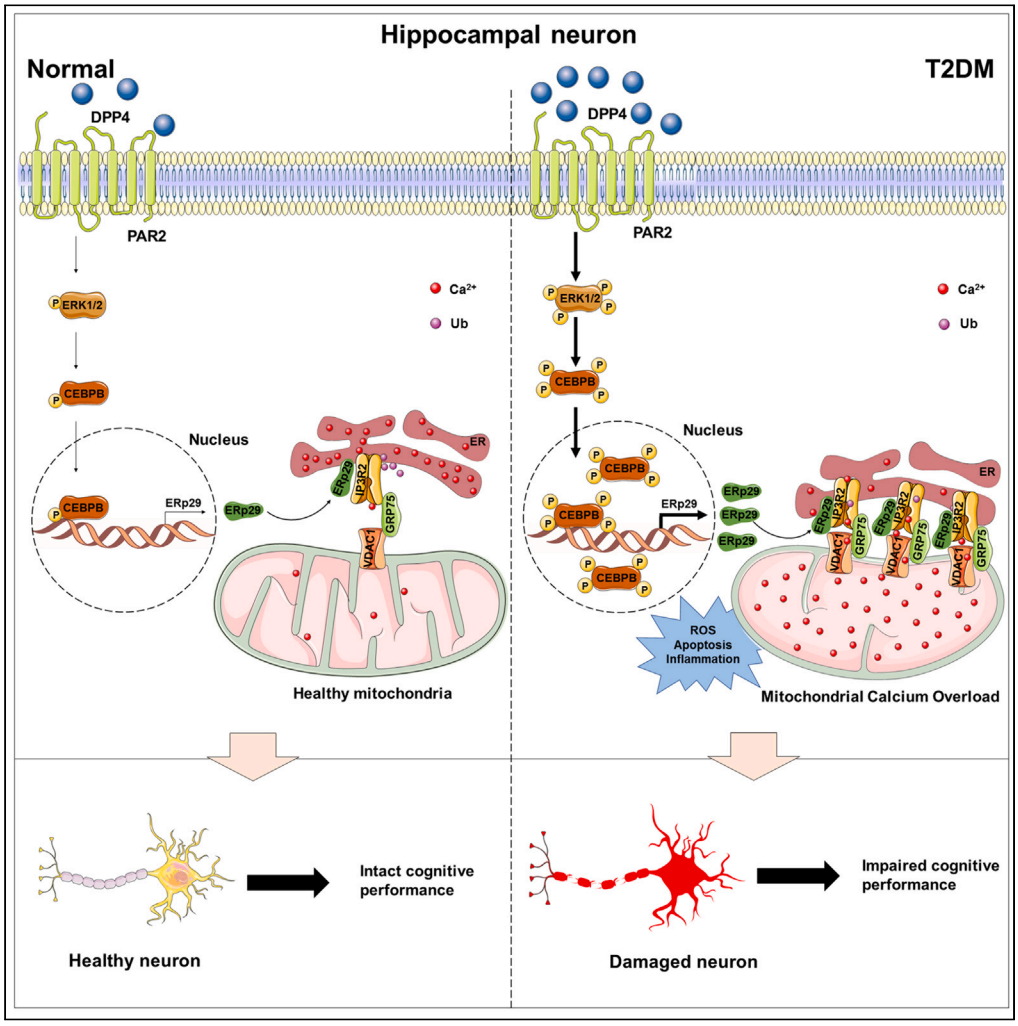

Jiaxiu Li, Ya Hui, Zhiqiang Xu, ..., Junjie Wei, Qiongsui Zhong, Tianpeng Zheng

w19831120@126.com

Highlights

DPP4 impairs hippocampal neurons and leads to cognitive dysfunction

DPP4 induces mitochondrial calcium overload in hippocampal neurons

PAR2/ERK1/2/CEBPB/ERp29 signaling is involved in DPP4-induced effects

DPP4 activates this pathway in an enzymatic activity-independent manner

Li et al., iScience 26, 106271
March 17, 2023 © 2023 The Author(s).
https://doi.org/10.1016/j.isci.2023.106271

iScience

CellPress
OPEN ACCESS

Article

Non-canonical function of DPP4 promotes cognitive impairment through ERp29-associated mitochondrial calcium overload in diabetes

Jiaxiu Li,[1,2,3,6] Ya Hui,[1,2,6] Zhiqiang Xu,[1,2,6] Jie Tan,[3] Kai Yin,[2] Liuyu Kuang,[1,2] Yunyun Tang,[1,2] Junjie Wei,[5] Qiongsui Zhong,[5] and Tianpeng Zheng[1,2,3,4,7,*]

SUMMARY

DPP4 has been shown to induce diabetes-associated mitochondrial dysfunction and cognitive impairment through its non-canonical function. Here, we report that enhanced DPP4 expression in diabetes contributes to IP3R2-mediated mitochondria-associated ER membrane (MAM) formation, mitochondria calcium overload, and cognitive impairment, and its knockdown showed opposite effects. Mechanistically, DPP4 binds to PAR2 in hippocampal neurons and activates ERK1/2/CEBPB signaling, which upregulates ERp29 expression and promotes its binding to IP3R2, thereby inhibiting IP3R2 degradation and promoting MAM formation, mitochondria calcium overload, and cognitive impairment. Meanwhile, targeting DPP4-mediated PAR2/ERK1/2/CEBPB/ERp29 signaling achieved satisfactory therapeutic effects on MAM formation, mitochondria calcium overload, and cognitive impairment. Notably, DPP4 activates this pathway in an enzymatic activity-independent manner, suggesting the non-canonical role of DPP4 in the pathogenesis of mitochondria calcium overload and cognitive impairment in diabetes. Together, these results identify DPP4-mediated PAR2/ERK1/2/CEBPB/ERp29 signaling as a promising therapeutic target for the treatment of cognitive impairment in type 2 diabetes.

INTRODUCTION

Cognitive impairment is increasingly recognized as an important complication of type 2 diabetes.[1] It has been reported that type 2 diabetes is associated with a 2-2.5 times increased risk of mild cognitive impairment and 1.5-times increased risk of dementia.[1,2] Moreover, previous studies have shown that neuroinflammation and oxidative stress induced by hyperglycemia contributes to the deterioration of mitochondrial function, which further promotes the onset and development of cognitive impairment.[3–5] Although mitochondrial dysfunction is implicated in the pathophysiology of diabetes-associated cognitive impairment, the underlying mechanism for such effects remains unclear.

Mitochondria play a vital role in the regulation of many cellular functions, including Ca^{2+} homeostasis, energy production, mitophagy, lipid synthesis, protein folding, apoptosis, and so forth. These functions require a dynamic spatial organization that regulates signal transduction between mitochondria and other organelles. In particular, mitochondria communicate with ER through specialized contacts sites known as mitochondria-associated ER membrane (MAM), which link both organelles through proteinaceous tethers. For example, the vesicle-associated membrane protein-associated protein B (VAPB) tethers the ER to mitochondria by forming complexes with mitochondrial protein tyrosine phosphatase interacting protein 51 (PTPIP51). Voltage-dependent anion-selective channel 1 (Vdac1) interacts with inositol 1,4,5-trisphosphate receptors (Ip3rs) to form calcium tunnel between mitochondria and ER.[6,7] Alterations in MAM formation have pleiotropic effects on multiple diseases, such as neurodegenerative diseases,[8] diabetic cardiomyopathy,[9] neoangiogenesis[10] and virus infection.[11] Additionally, increasing evidence highlight that increased MAM formation induced mitochondria dysfunction through mitochondria calcium overload. The Ip3r-Grp75-VDAC1 complex in MAM is the main factor responsible for Ca^{2+} release from ER to mitochondria. Moderate Ca^{2+} transfer is essential to maintain mitochondrial oxidative metabolism and energy production; however, prolonged mitochondrial calcium overload induced by increased Ip3r-Grp75-VDAC1 complex impairs mitochondrial function by causing the

[1]Department of Endocrinology and Metabolism, The Second Affiliated Hospital of Guilin Medical University, Guilin, Guangxi 541199, P. R. China

[2]Guangxi Key Laboratory of Diabetic Systems Medicine, Guilin Medical University, Guilin, Guangxi 541199, P. R. China

[3]Guangxi Key Laboratory of Brain and Cognitive Neuroscience, Guilin Medical University, Guilin, Guangxi 541199, P. R. China

[4]Guangxi Health Commission Key Laboratory of Glucose and Lipid Metabolism Disorders, The Second Affiliated Hospital of Guilin Medical University, Guilin, Guangxi 541199, P. R. China

[5]Lingui Clinical Medical College, Guilin Medical University, Guilin, Guangxi 541199, P. R. China

[6]These authors contributed equally

[7]Lead contact

*Correspondence: w19831120@126.com

https://doi.org/10.1016/j.isci.2023.106271

This is an open access article under the CC BY-NC-ND license (http://creativecommons.org/licenses/by-nc-nd/4.0/).

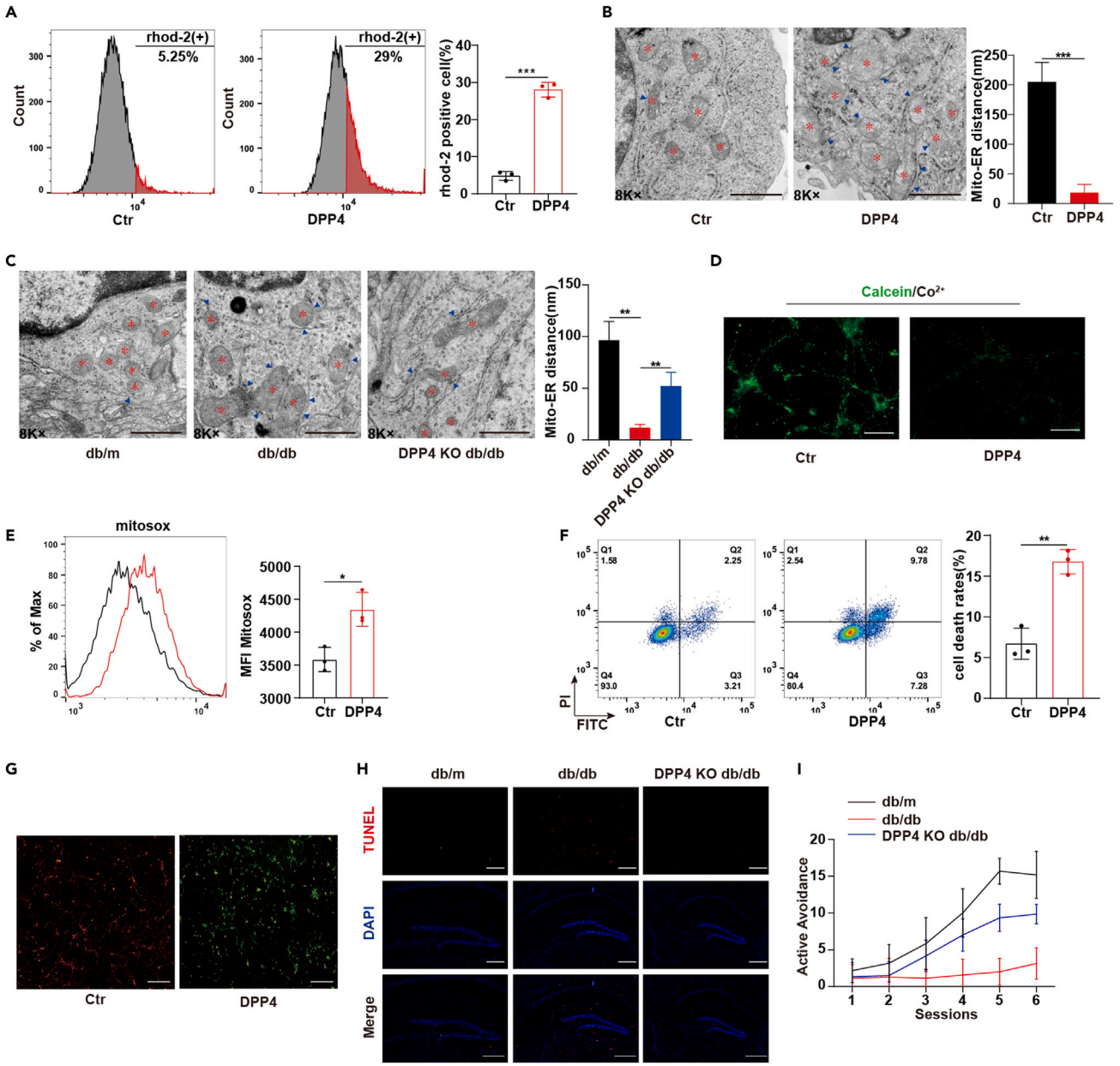

Figure 1. DPP4 induces MAM formation and mitochondrial calcium overload, impairs mitochondria function and leads to cognitive impairment

(A) Flow cytometry analysis (FCM) using Rhod-2 revealed mitochondrial calcium levels in primary hippocampal neurons treated with or without DPP4 (500 ng/mL) for 24 h. Quantitative data show the percentage of Rhod-2 positive cells.

(B) Representative transmission electron microscope (TEM) images of the ER and mitochondrial morphology in primary hippocampal neurons treated with or without DPP4 (500 ng/mL) for 24 h. The red asterisks indicate mitochondria, and the blue triangles indicate ER. Scale bar, 1 μm.

(C) Representative TEM images of the ER and mitochondrial morphology in the hippocampus of db/m, db/db, and DPP4 KO db/db mice. The red asterisks indicate mitochondria, and the blue triangles indicate ER. Scale bar, 1 μm.

(D) Monitoring the opening of MPTP in primary hippocampal neurons treated with or without DPP4 (500 ng/mL) for 24 h. Cells were loaded with calcein-AM in the presence of Co^{2+}.

(E) FCM analysis of reactive oxygen species (ROS) levels in primary hippocampal neurons treated with or without DPP4 (500 ng/mL) for 24 h. Quantitative data show the percentage of ROS levels.

(F) FCM analysis of apoptosis in primary hippocampal neurons treated with or without DPP4 (500 ng/mL) for 24 h. Quantitative data show the percentage of cell death rates.

CellPress
OPEN ACCESS

Figure 1. *Continued*
(G) Mitochondrial membrane potential (MMP) measurement using JC-1 dye in primary hippocampal neurons treated with or without DPP4 (500 ng/mL) for 24 h.
(H) Representative images of sections of the hippocampus from db/m, db/db, and DPP4 KO db/db mice subjected to TUNEL staining (red).
(I) The active avoidance performance of db/m, db/db, or DPP4 KO db/db mice (n = 6/group).

collapse of the mitochondrial membrane potential, leading to long-time mitochondrial permeability transition pore (MPTP) opening, mtDNA leakage and apoptosis.[10,12,13]

Dipeptidyl peptidase-4 (DPP4) is a ubiquitous serine exopeptidase existing as either a membrane-anchored cell surface protein or as a soluble form that retains extracellular domains and catalytic activity. The enzymatic function of DPP4 enables cleavage of X-proline dipeptides from the N terminus of polypeptide substrates.[5,14,15] In addition to its well-known enzymatic function, DPP4 also possesses non-canonical functions through its interaction with ligands or receptors including fibronectin, adenosine deaminase and protease-activated receptor2 (PAR2).[16] Increased DPP4 activity has been proved to be an independent risk factor for mild cognitive impairment in patients with type 2 diabetic [2,5,17]; however, findings supporting the association between DPP4 activity inhibitors and improvement in cognition impairment are inconsistent in type 2 diabetes. In some studies, DPP4 inhibitors have been proven to ameliorate cognitive impairment in patients with elderly diabetics,[18,19] whereas another study by Biessels et al. found no apparent association between DPP4 inhibitors and improvement of cognitive function in a large international randomized trial in people with type 2 diabetes.[20] Interestingly, our group recently reported that DPP4 can modulate GSK-3β/PGC-1α signaling pathway through interacting with PAR2, initiate mitochondrial dysfunction and lead to cognitive impairment in db/db mice, more importantly, the inhibition of DPP4 activity did not restore mitochondrial dysfunction induced by DPP4 in primary hippocampal neurons, suggesting the non-canonical function of DPP4 in the pathogenesis of mitochondrial dysfunction and cognitive impairment in type 2 diabetes. However, the possible role of DPP4 in regulating MAM formation and mitochondrial calcium overload in diabetes-associated cognitive impairment remains largely unknown.

In this study, we demonstrated that the DPP4-mediated PAR2/ERK/CEBPB/ERp29 signaling pathway inhibited IP3R2 degradation, resulting in increased MAM formation, mitochondrial calcium overload, mitochondrial dysfunction and finally leading to cognitive impairment in diabetes. Additionally, DPP4 mediates these effects in an enzymatic activity-independent manner, representing a potential therapeutic target for cognitive impairment intervention in type 2 diabetes.

RESULTS

DPP4 induces mitochondria-associated endoplasmic reticulum membrane formation and mitochondrial calcium overload, impairs mitochondria function, and leads to cognitive impairment

Mitochondrial calcium overload is an important mechanism that contributes to mitochondrial dysfunction.[21] Therefore, we determined the impact of DPP4 on mitochondrial calcium levels. To this end, the mitochondrial Ca^{2+} indicator, Rhod-2, AM was used to determine mitochondrial Ca^{2+} levels based on the flow cytometer. The AM ester forms of Rhod-2 are cationic, resulting in potential-driven uptake into mitochondria. This has led to the use of Rhod-2 as a selective indicator for mitochondrial Ca^{2+}.[22] As shown in Figure 1A, DPP4 treatment for 24 h increased rhod-2-positive cell population in primary hippocampal neurons, which indicates DPP4 induces mitochondrial calcium influx. Mitochondria-associated ER membrane (MAM) is a site of physiological communication between mitochondria and the ER, which controls calcium transport from the ER to mitochondria.[6] We, therefore, examined whether DPP4 could induce MAM formation, transmission electron microscopy (TEM) images showed that DPP4 treatment enhanced the percentage of ER adjacent to mitochondria in primary hippocampal neurons (Figure 1B). Next, we assessed the effects of DPP4 knockout on MAM formation in db/db hippocampus. As illustrated by TEM images (Figure 1C), the association between the ER and mitochondria was significantly increased in the hippocampus of db/db mice and this increased association was prevented by DPP4 knockout in db/db mice. Therefore, these results demonstrate that DPP4 contributes to hippocampal MAM formation and mitochondrial Ca^{2+} increase in type 2 diabetes.

Next, we examined the effects of DPP4 on mitochondrial function both *in vivo* and *in vitro*. As expected, DPP4 treatment significantly increased MPTP opening (Figure 1D), ROS generation (Figure 1E), and

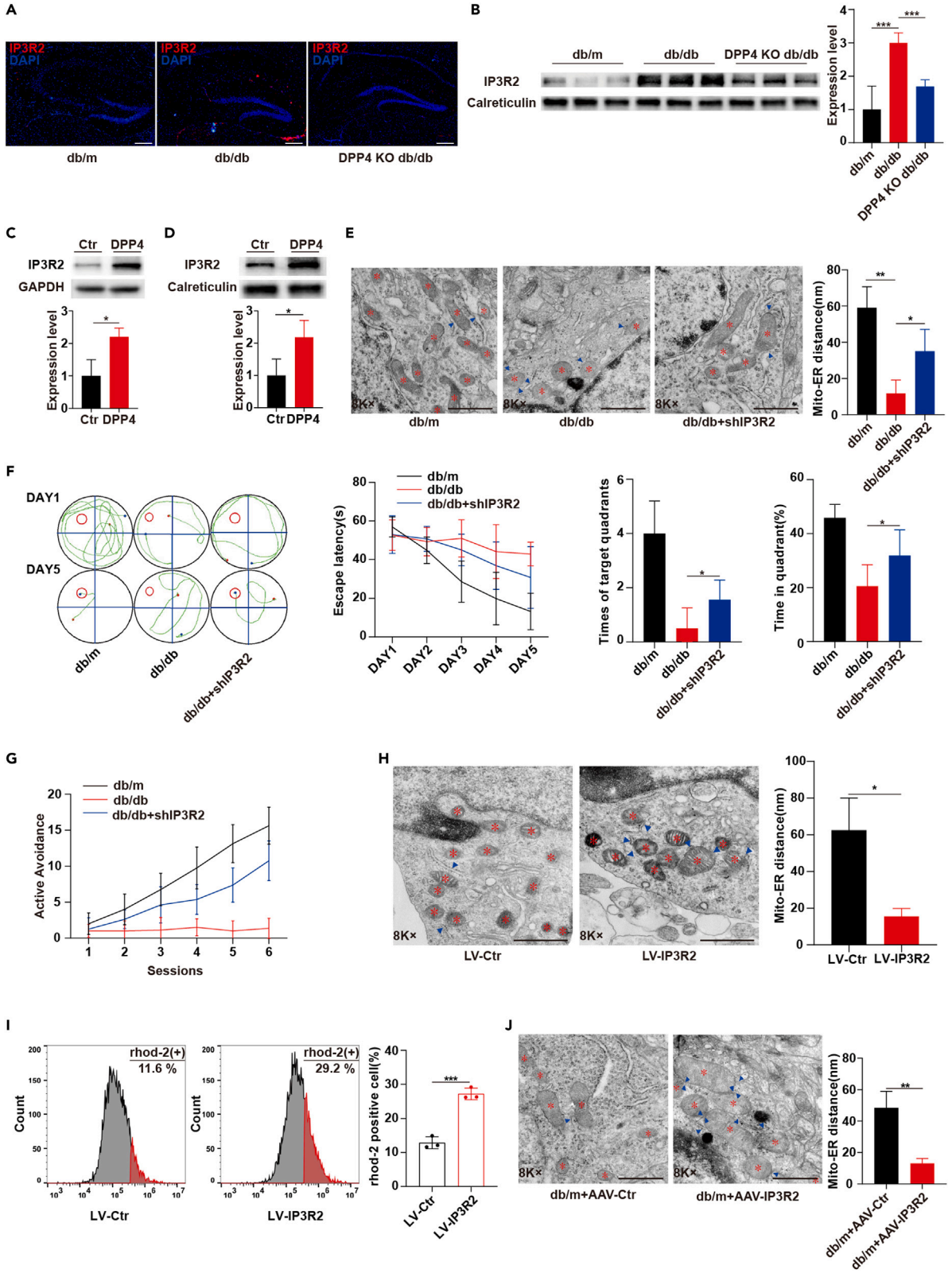
A
IP3R2
DAPI
db/m
db/db
DPP4 KO db/db
B
db/m
db/db
DPP4 KO db/db
IP3R2
Calreticulin
Expression level
C
Ctr
DPP4
IP3R2
GAPDH
Expression level
Ctr DPP4
D
Ctr
DPP4
IP3R2
Calreticulin
Expression level
Ctr DPP4
E
8K×
db/m
db/db
db/db+shIP3R2
Mito-ER distance(nm)
F
DAY1
DAY5
db/m
db/db
db/db+shIP3R2
Escape latency(s)
DAY1
DAY2
DAY3
DAY4
DAY5
Times of target quadrants
Time in quadrant(%)
G
Active Avoidance
Sessions
H
LV-Ctr
LV-IP3R2
Mito-ER distance(nm)
I
rhod-2(+)
11.6 %
rhod-2(+)
29.2 %
Count
LV-Ctr
LV-IP3R2
rhod-2 positive cell(%)
J
db/m+AAV-Ctr
db/m+AAV-IP3R2
Mito-ER distance(nm)

Figure 2. IP3R2 expression is up-regulated by DPP4 and contributes to MAM formation, mitochondrial dysfunction, and cognitive impairment

(A) Representative images for IP3R2 (red) in the hippocampus of db/m, db/db, and DPP4 KO db/db mice. (n = 6/group).

(B) Immunoblots and quantification analysis of protein level of IP3R2 in MAM fraction isolated from db/m, db/db, and DPP4 KO db/db mice hippocampus (n = 6/group).

(C) Immunoblots and quantification analysis of protein level of IP3R2 in primary hippocampal neurons treated with or without DPP4 (500 ng/mL) for 24 h.

(D) Immunoblots and quantification analysis of protein level of IP3R2 in MAM fraction isolated from primary hippocampal neurons treated with or without DPP4 (500 ng/mL) for 24 h.

(E) Representative TEM images of the ER and mitochondrial morphology in the hippocampus of db/m, db/db, and db/db+shIP3R2 mice. The red asterisks indicate mitochondria, and the blue triangles indicate ER. Scale bar, 1 μm.

(F) Morris water maze behavioral assessment for db/m, db/db, or db/db+shIP3R2 mice showing differences in path (left), escape latency (second from left), number of times mice passed through the platform location in the probe trial (second from right) and the time mice stayed in the target quadrant (right) during the learning session. (n = 6/group).

(G) The active avoidance performance of db/m, db/db or db/db+shIP3R2 mice (n = 6/group).

(H) Representative TEM images of the ER and mitochondrial morphology in primary hippocampal neurons infected with IP3R2-overexpressing lentivirus or control lentivirus for 72 h. The red asterisks indicate mitochondria, and the blue triangles indicate ER. Scale bar, 1 μm.

(I) FCM analysis of mitochondrial calcium levels in primary hippocampal neurons infected with IP3R2-overexpressing lentivirus or control lentivirus for 72 h.

(J) Representative TEM images of the ER and mitochondrial morphology in the hippocampus of db/m and db/m+AAV-IP3R2 mice. The red asterisks indicate mitochondria, and the blue triangles indicate ER. Scale bar, 1 μm.

apoptosis (Figure 1F), and these effects were associated with a decrease in mitochondrial genes expressions (COI, CYTB, ND6, RNR2) (Figure S1A), mitochondrial membrane potential (MMP) levels (Figure 1G) and ATP productions (Figure S1B) in primary hippocampal neurons. Similarly, db/db mice exhibited increased inflammatory gene expression (Figure S1C), ROS generation (Figure S1D), and apoptosis (Figure 1H) but decreased mitochondrial genes expressions (Figure S1E), MMP levels (Figure S1F) and ATP productions (Figure S1G) in their hippocampus compared with db/m mice, whereas DPP4 knockout significantly reversed these effects and successfully improved cognitive function in db/db mice (Figures 1I and S1H). Taken together, our results demonstrate that DPP4 induces MAM formation and mitochondrial calcium overload, impairs mitochondrial function, and leads to cognitive impairment.

IP3R2 expression is up-regulated by DPP4 and contributes to mitochondria-associated endoplasmic reticulum membrane formation, mitochondrial dysfunction, and cognitive impairment

IP3R2 interacts with the voltage-dependent anion-selective channel 1 (VDAC1) to form an ER-mitochondria calcium tunnel and lead to calcium influx from the ER to mitochondria.[21] To examine whether IP3R2 is involved in DPP4-induced MAM formation and mitochondrial calcium overload, IP3R2 expression was determined in the hippocampus of db/m, db/db, and DPP4 KO db/db mice. As shown in Figures 2A and S2A, IP3R2 protein levels were significantly higher in the hippocampus from db/db mice compared to that in db/m nondiabetic mice, whereas DPP4 knockout in db/db mice significantly inhibited IP3R2 expression in the hippocampus. These results were similar when we examined the expression of IP3R2 in the MAM fraction isolated from mouse hippocampus (Figure 2B). The purity of the MAM fraction was demonstrated in Figure S2B. Next, we examined the effects of DPP4 on the expression of IP3R2 in primary hippocampal neurons. As expected, DPP4 treatment significantly increased IP3R2 expression in both hippocampal homogenates and hippocampal MAM fractions (Figures 2C and 2D), which further confirmed the *in vivo* findings that DPP4 upregulated the expression of IP3R2. In addition, we also found a significant increase in IP3R1 expression in MAM after DPP4 treatment (Figure S2C).

Next, we compared MAM formation in WT and IP3R2 knockdown hippocampus of db/db. As demonstrated by TEM (Figure 2E), IP3R2 knockdown (KD) significantly reduced the association between mitochondria and ER in the hippocampus of db/db mice. We further determined whether IP3R2 mediated mitochondrial dysfunction under diabetic conditions. As shown in Figures S2D–S2J, IP3R2 knockdown (Figure S2D) significantly decreased inflammatory gene expression (Figure S2E), ROS generation (Figure S2F), apoptosis (Figure S2G) and increased mitochondrial genes expressions (Figure S2H), MMP levels (Figure S2I) and ATP productions (Figure S2J). To explore if mitochondrial dysfunction was correlated with cognitive impairment, we next evaluated the effects of IP3R2 knockdown on spatial learning and memory performance using context fear conditioning tests and water maze tests. As shown in Figures 2F and 2G, the cognitive function of db/db mice was worse than that of the db/m mice, and IP3R2 KD significantly improved such deficits in db/db mice.

To further assess the effect of IP3R2 on MAM formation, mitochondrial calcium overload, and mitochondrial dysfunction *in vitro*, mouse primary hippocampal neurons were infected with lentivirus

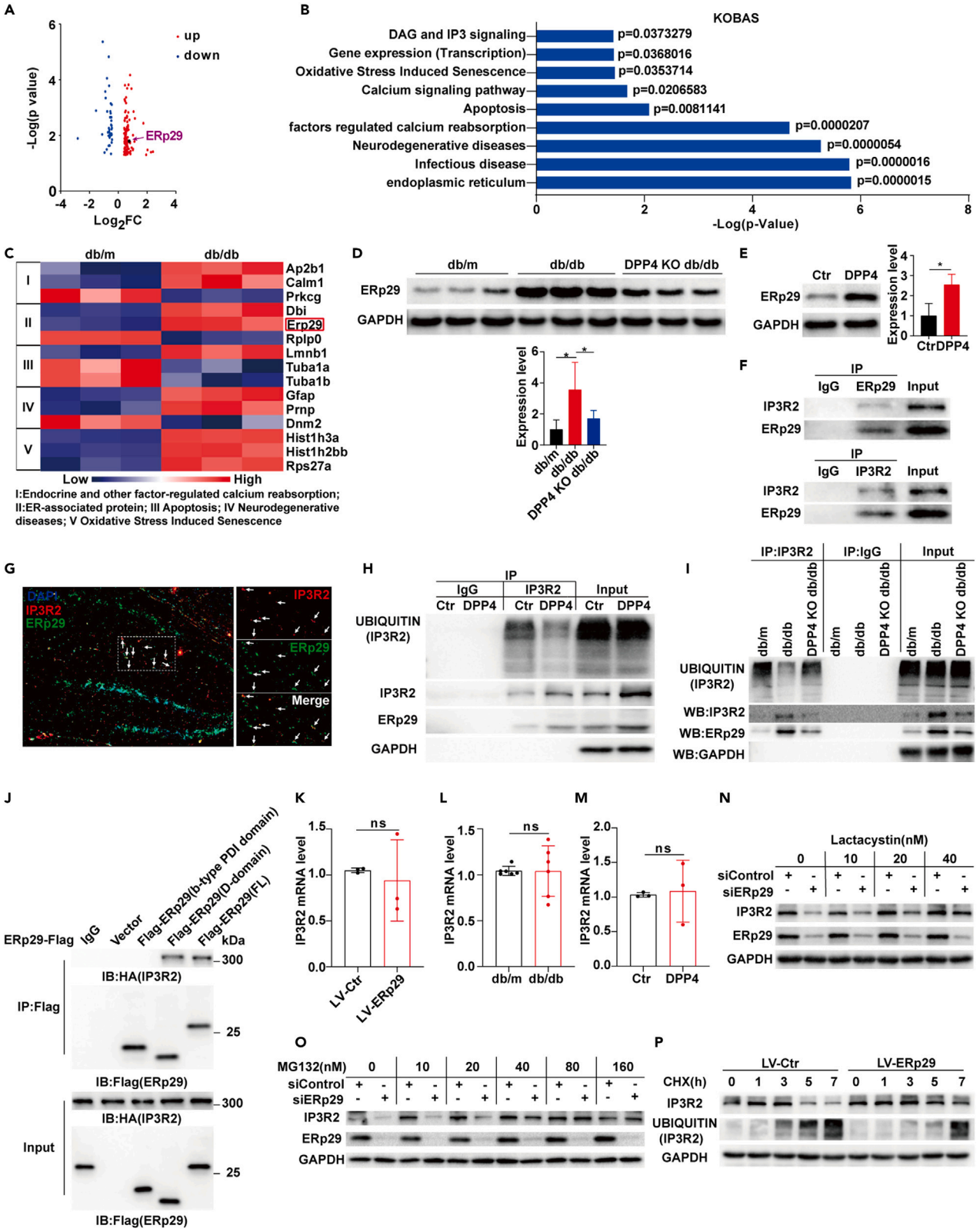
A
up
down
ERp29
-Log(p value)
Log2FC
B
KOBAS
DAG and IP3 signaling p=0.0373279
Gene expression (Transcription) p=0.0368016
Oxidative Stress Induced Senescence p=0.0353714
Calcium signaling pathway p=0.0206583
Apoptosis p=0.0081141
factors regulated calcium reabsorption p=0.0000207
Neurodegenerative diseases p=0.0000054
Infectious disease p=0.0000016
endoplasmic reticulum p=0.0000015
-Log(p-Value)
C
db/m
db/db
Ap2b1
Calm1
Prkcg
Dbi
Erp29
Rplp0
Lmnb1
Tuba1a
Tuba1b
Gfap
Prnp
Dnm2
Hist1h3a
Hist1h2bb
Rps27a
Low
High
I:Endocrine and other factor-regulated calcium reabsorption; II:ER-associated protein; III Apoptosis; IV Neurodegenerative diseases; V Oxidative Stress Induced Senescence
D
db/m
db/db
DPP4 KO db/db
ERp29
GAPDH
Expression level
E
Ctr
DPP4
ERp29
GAPDH
Expression level
F
IP
IgG
ERp29
Input
IP3R2
IP
IgG
IP3R2
Input
G
DAPI
IP3R2
ERp29
Merge
H
IP
IgG
IP3R2
Input
Ctr
DPP4
UBIQUITIN (IP3R2)
IP3R2
ERp29
GAPDH
I
IP:IP3R2
IP:IgG
Input
db/m
db/db
DPP4 KO db/db
UBIQUITIN (IP3R2)
WB:IP3R2
WB:ERp29
WB:GAPDH
J
ERp29-Flag
IgG
Vector
Flag-ERp29(b-type PDI domain)
Flag-ERp29(D-domain)
Flag-ERp29(FL)
kDa
300
IB:HA(IP3R2)
IP:Flag
25
IB:Flag(ERp29)
300
IB:HA(IP3R2)
Input
25
IB:Flag(ERp29)
K
IP3R2 mRNA level
ns
LV-Ctr
LV-ERp29
L
IP3R2 mRNA level
ns
db/m
db/db
M
IP3R2 mRNA level
ns
Ctr
DPP4
N
Lactacystin(nM)
0
10
20
40
siControl
siERp29
IP3R2
ERp29
GAPDH
O
MG132(nM)
0
10
20
40
80
160
siControl
siERp29
IP3R2
ERp29
GAPDH
P
LV-Ctr
LV-ERp29
CHX(h)
0
1
3
5
7
IP3R2
UBIQUITIN (IP3R2)
GAPDH

Figure 3. DPP4 upregulates ERp29 expression, promotes its binding to IP3R2 and inhibits IP3R2 proteasomal degradation

(A) The volcano plot indicated differentially expressed proteins. The red dots represented up-regulated proteins, while the blue dots represented down-regulated proteins. ERp29 is one of the up-regulated proteins.

(B) Differentially expressed proteins (>1.2-fold) were grouped into gene pathways using the pathway enrichment analysis with KOBAS software.

(C) Heatmap of differentially expressed proteins in the brain MAM of db/db mice compared with db/m mice. Relative expression is depicted in red (high expression) or blue (low expression) for each protein.

(D) Immunoblots and quantification analysis of protein level of ERp29 in the hippocampus from db/m, db/db, or DPP4 KO db/db mice (n = 6/group).

(E) Immunoblots and quantification analysis of protein level of ERp29 in primary hippocampal neurons treated with or without DPP4 (500 ng/mL) for 24 h.

(F) The interaction between ERp29 and IP3R2 in primary hippocampal neurons was detected by immunoprecipitation and western blot.

(G) Double immunofluorescence demonstrates the co-localization of IP3R2 and ERp29 in the hippocampus from db/db mice; arrowheads indicate the co-localization of IP3R2 and ERp29.

(H and I) Results of IP experiments in primary hippocampal neurons treated with or without DPP4 (H), in the hippocampus of db/m, db/db, and DPP4 KO db/db mice (I). Anti-IP3R2 IP was followed by western blotting for ubiquitin to determine levels of ubiquitin-IP3R2. The protein levels of IP3R2 and ERp29 in the precipitates were determined with protein-specific primary antibodies.

(J) Interactions between IP3R2 and ERp29 (full length), the ERp29 (b-type PDI domain), or the ERp29 (D-domain) in 293T cells were determined by co-IP.

(K) mRNA levels of IP3R2 in primary hippocampal neurons infected with ERp29-overexpressing lentivirus or control lentivirus for 72 h were measured by RT-PCR.

(L) mRNA levels of IP3R2 in the hippocampus of db/m and db/db mice were measured by RT-PCR.

(M) mRNA levels of IP3R2 in primary hippocampal neurons treated with or without DPP4 were measured by RT-PCR.

(N and O) Western blot analysis for IP3R2 and ERp29 in primary hippocampal neurons transfected with control siRNA (siControl) or ERp29 siRNA for 48h and treated with Lactacystin (N) or MG132 (O) at the indicated dose.

(P) Western blot analysis of IP3R2 in primary hippocampal neurons infected with LV-ERp29 for 48h, and treated with 200 μmol/L of cycloheximide (CHX) for the indicated time.

overexpressing IP3R2 or containing control vector (Figure S3A). As expected, IP3R2 overexpression significantly increased MAM formation (Figure 2H) and mitochondrial Ca^{2+} concentrations (Figure 2I), and these effects were associated with a decrease in mitochondria genes expression (Figure S3B), MMP levels (Figure S3C), ATP production (Figure S3D) and an increase in MPTP opening (Figure S3E), ROS generation (Figure S3F) and apoptosis (Figure S3G). Similarly, IP3R2 overexpression (Figure S3H) in the hippocampus of db/m mice significantly induced MAM formation (Figure 2J), impaired mitochondria function (Figures S3I–S3M), and lead to cognitive impairment (Figures S3O and S3P).

DPP4 upregulates ERp29 expression, promotes its binding to IP3R2 and inhibits IP3R2 proteasomal degradation

To further understand the changes of MAM-related proteins in diabetes, we used a published dataset to analyze the proteome profiling of isolated brain MAM from db/m nondiabetic and db/db type 2 diabetic mice.[23] All the relevant data in the present study were downloaded from https://www.nature.com/articles/s41598-017-02213-1#Sec22. In this datasets, a total of 1,313 non-redundant proteins of MAM were identified, among which 144 proteins were found significantly altered in diabetes. Volcano plot represented the expression changes of all proteins (Figure 3A). Then, we selected those differentially expressed proteins for GO annotation and pathway analysis. Up- and downregulated proteins were related to calcium reabsorption (Gnal, Asph, Prkcg, Calm1, Dnm1, Ap2a1, Ap2b1, Prkcg, Dnm2), ER-associated proteins (Dbi, Asph, Slc9a1, Lrpap1, Alb, Calr, Rplp0, Prnp, Nrxn1, Vcp, Olfm1, Gdpd1, Chp1, Erp29, Ass1, P4hb, Prkcsh), apoptosis (Tuba4a, Tuba1a, Lmnb1, Tuba1b), neurodegenerative diseases (Tuba4a, Slc9a1, Dnm2, Uba1, Prnp, Prkcg, Vcp, Plp1, Ndrg1, Gfap) and oxidative stress-induced senescence (Hist1h3a, Hist1h2bb, Rps27a) (Figure 3B). Similar results were obtained using heat maps (http://kobas.cbi.pku.edu.cn/kobas3/genelist/) (Figure 3C). Since the expression and function of IP3R2 were shown to be assisted by various molecular chaperones,[24,25] we next tested whether molecular chaperones were differentially expressed in MAM. Notably, ER protein 29 (ERp29), a non-classical molecular chaperone of the ER that plays a pleiotropic role in regulating biosynthesis and transport of transmembrane and secretory proteins,[26] were found to be upregulated in the brain MAM of db/db mice (Figures 3A and 3C). To confirm this finding, we also examined ERp29 protein expression in the hippocampus MAM collected from db/m nondiabetic and db/db type 2 diabetic mice. As depicted in Figure 3D, ERp29 levels were significantly increased in hippocampus from db/db mice compared to those in nondiabetic db/m controls and DPP4 deletion successfully reversed this increase in ERp29 expression in db/db mice. Similarly, this increase was also observed in primary hippocampal neurons treated with DPP4 as compared to controls (Figure 3E). Taken together, we concluded that DPP4 upregulated ERp29 protein expression in the hippocampal MAM.

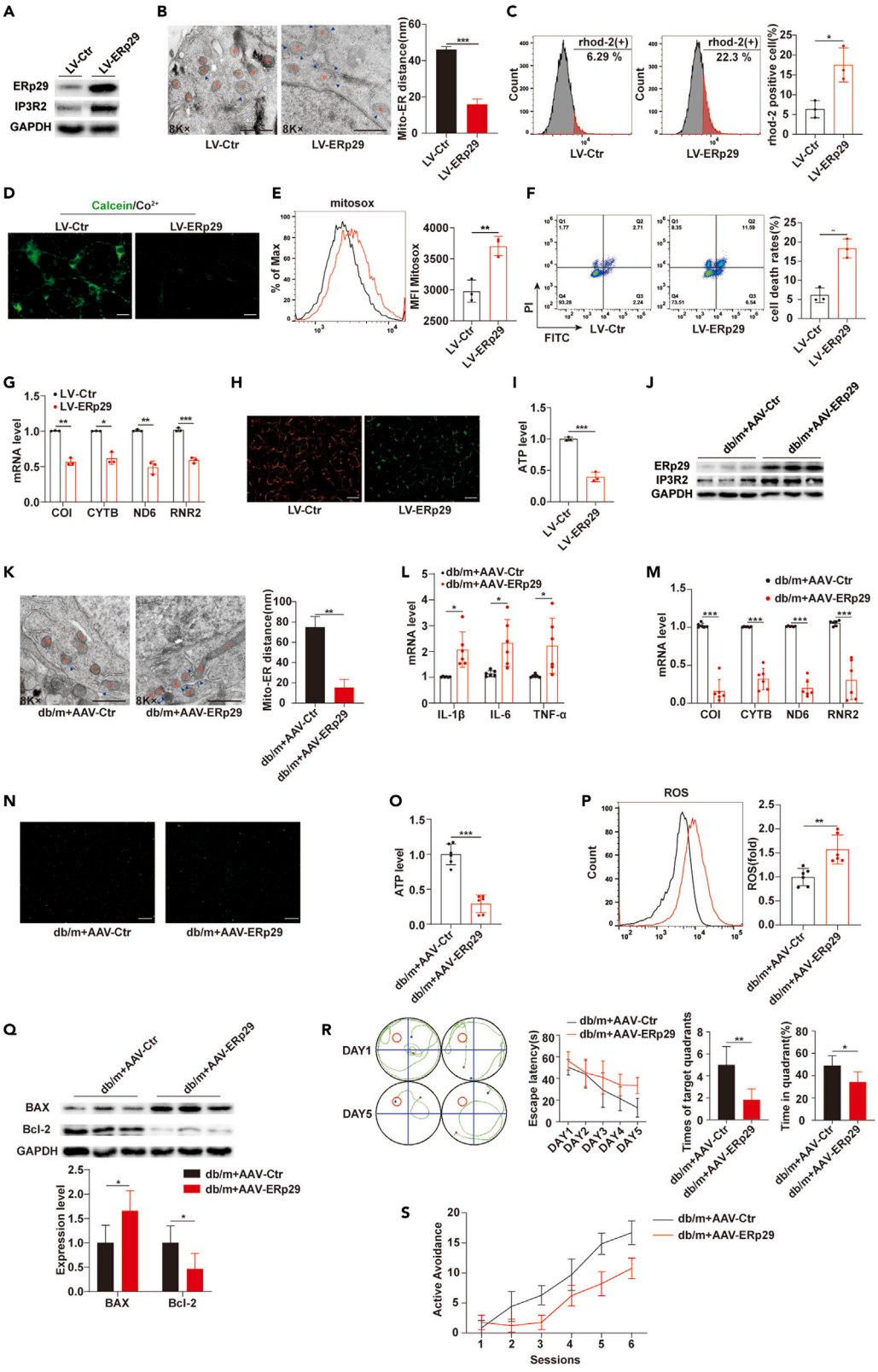
A
LV-Ctr
LV-ERp29
ERp29
IP3R2
GAPDH
B
8K×
LV-Ctr
LV-ERp29
Mito-ER distance(nm)
C
rhod-2(+)
6.29 %
rhod-2(+)
22.3 %
Count
rhod-2 positive cell(%)
D
Calcein/Co2+
LV-Ctr
LV-ERp29
E
mitosox
% of Max
MFI Mitosox
F
PI
FITC
cell death rates(%)
G
LV-Ctr
LV-ERp29
mRNA level
COI
CYTB
ND6
RNR2
H
LV-Ctr
LV-ERp29
I
ATP level
J
db/m+AAV-Ctr
db/m+AAV-ERp29
ERp29
IP3R2
GAPDH
K
db/m+AAV-Ctr
db/m+AAV-ERp29
Mito-ER distance(nm)
L
db/m+AAV-Ctr
db/m+AAV-ERp29
mRNA level
IL-1β
IL-6
TNF-α
M
db/m+AAV-Ctr
db/m+AAV-ERp29
mRNA level
COI
CYTB
ND6
RNR2
N
db/m+AAV-Ctr
db/m+AAV-ERp29
O
ATP level
P
ROS
Count
ROS(fold)
Q
db/m+AAV-Ctr
db/m+AAV-ERp29
BAX
Bcl-2
GAPDH
Expression level
R
DAY1
DAY5
Escape latency(s)
DAY1
DAY2
DAY3
DAY4
DAY5
Times of target quadrants
Time in quadrant(%)
S
Active Avoidance
Sessions

Figure 4. Hippocampal overexpression of ERp29 promotes MAM formation, mitochondrial calcium overload, impairs mitochondrial function and leads to cognitive impairment

(A–I) Immunoblots analysis of protein levels of ERp29, IP3R2 (A), representative TEM images of the ER and mitochondrial morphology (Scale bar, 1 μm) (B), FCM analysis of mitochondrial calcium levels (C), MPTP opening (D), ROS level (E), apoptosis level (F), mRNA levels of mitochondrial functional genes COI, CYTB, ND6, RNR2 (G), MMP (H), and ATP level (I) in primary hippocampal neurons infected with ERp29-overexpressing lentivirus or control lentivirus for 72 h.

(J–Q) Immunoblots analysis of protein levels of ERp29, IP3R2 (J), representative TEM images of the ER and mitochondrial morphology (Scale bar, 1 μm) (K), mRNA levels of inflammatory factors IL-1β, IL-6, TNF-α (L), mRNA levels of mitochondrial functional genes COI, CYTB, ND6, RNR2 (M), MMP (N), ATP level (O), ROS level (P), and immunoblots and quantification analysis of protein levels of BAX and Bcl-2 (Q) in the hippocampus from db/m and db/m+AAV-ERp29 mice. (n = 6/group).

(R) Morris water maze behavioral assessment for db/m and db/m+ AAV-ERp29 mice showing differences in path (left), escape latency (second from left), number of times mice passed through the platform location in the probe trial (second from right) and the time mice stayed in the target quadrant (right) during the learning session. (n = 6/group).

(S) The active avoidance performance of db/m and db/m+ AAV-ERp29 mice. (n = 6/group).

Previous studies have proved that ERp29 regulates the biosynthesis and trafficking of several transmembrane and secretory proteins through its interactions with other receptors.[26] We, therefore, performed co-immuno- precipitation and immunofluorescence double staining experiments to test whether ERp29 could bind to IP3R2. As expected, ERp29 could be pulled down by using IP3R2 as the precipitating antibody in primary hippocampal neurons, and vice versa (Figure 3F). Meanwhile, the immunofluorescence detection showed the co-localization of ERp29 and IP3R2 *in vivo* (Figure 3G). Next, we evaluated if DPP4 could promote the binding of ERp29 and IP3R2 both *in vitro* and *in vivo*. As shown in Figure 3H, DPP4 treatment significantly decreased IP3R2 ubiquitination and increased the level of IP3R2 associated with ERp29 in primary hippocampal neurons. Consistent with our *in vitro* data, the formation of ERp29-IP3R2 complex was significantly increased in the hippocampus of db/db mice compared to controls and DPP4 deletion successfully reversed the increase in ERp29-IP3R2 complex expression (Figure 3I). Collectively, these results suggest that ERp29 can directly bind to IP3R2 and DPP4 facilitates the binding of ERp29 to IP3R2. ERp29 has an N-terminal domain (amino acids 7-29), b-type PDI domain (amino acids 35-157), D-domain (amino acids 159-252), and an ER retrieval KEEL domain at the C-terminus (amino acids 259-262).[26] To identify the specific regions of ERp29 that is responsible for the interaction between ERp29 and IP3R2, we expressed full-length HA-tagged IP3R2 in combination with different Flag-tagged fragments of ERp29 in HEK293 cells. As shown in Figure 3J, the D-domain of ERp29 containing substrate binding site showed a strong interaction, whereas the b-type PDI domain did not interact with IP3R2.

Based on the finding that ERp29 can directly bind to IP3R2, we next tested if the increased IP3R2 protein level in diabetes was the result of ERp29-mediated higher expression or reduced degradation. First, we determined if ERp29 overexpression in primary hippocampal neurons could alter IP3R2 mRNA levels. As shown in Figure 3K, ERp29 overexpression had no effect on IP3R2 mRNA expression, in addition, IP3R2 mRNA levels were unchanged in the hippocampus of db/db mice (Figure 3L) and DPP4-treated primary hippocampal neurons (Figure 3M), suggesting that DPP4-mediated binding of ERp29 to IP3R2 might affect IP3R2 protein expression by preventing its degradation. Therefore, we determined if ERp29 could prevent proteasome-mediated IP3R2 degradation. To this end, both control siRNA- and ERp29 siRNA-treated primary hippocampal neurons were treated with the lactacystin or proteasome inhibitor MG132 for 48 h. Either Lactacystin (Figure 3N) or MG132 (Figure 3O) treatment significantly reversed the reduction of IP3R2 induced by ERp29 silencing. In addition, ERp29 overexpression inhibited IP3R2 ubiquitination and its degradation (Figure 3P). Together, these findings demonstrated that ERp29 prevented proteasome-mediated IP3R2 degradation.

Hippocampal overexpression of ERp29 promotes mitochondria-associated endoplasmic reticulum membrane formation, mitochondrial calcium overload, impairs mitochondrial function, and leads to cognitive impairment

Since DPP4 upregulated ERp29 expression, we examined the impact of ERp29 overexpression on MAM formation, mitochondrial function, and cognitive ability. Primary hippocampal neurons infected with ERp29-expressing lentivirus (Figure 4A) exhibited increased MAM formation (Figure 4B), mitochondrial Ca^{2+} concentrations (Figure 4C), MPTP opening (Figure 4D), ROS generation (Figure 4E), apoptosis (Figure 4F) and decreased mitochondria genes expression (Figure 4G), MMP levels (Figure 4H), ATP production (Figure 4I), suggesting that ERp29 overexpression induced MAM formation and mitochondrial dysfunction. We also demonstrated these effects of ERp29 overexpression in WT and ERp29 overexpression hippocampus of

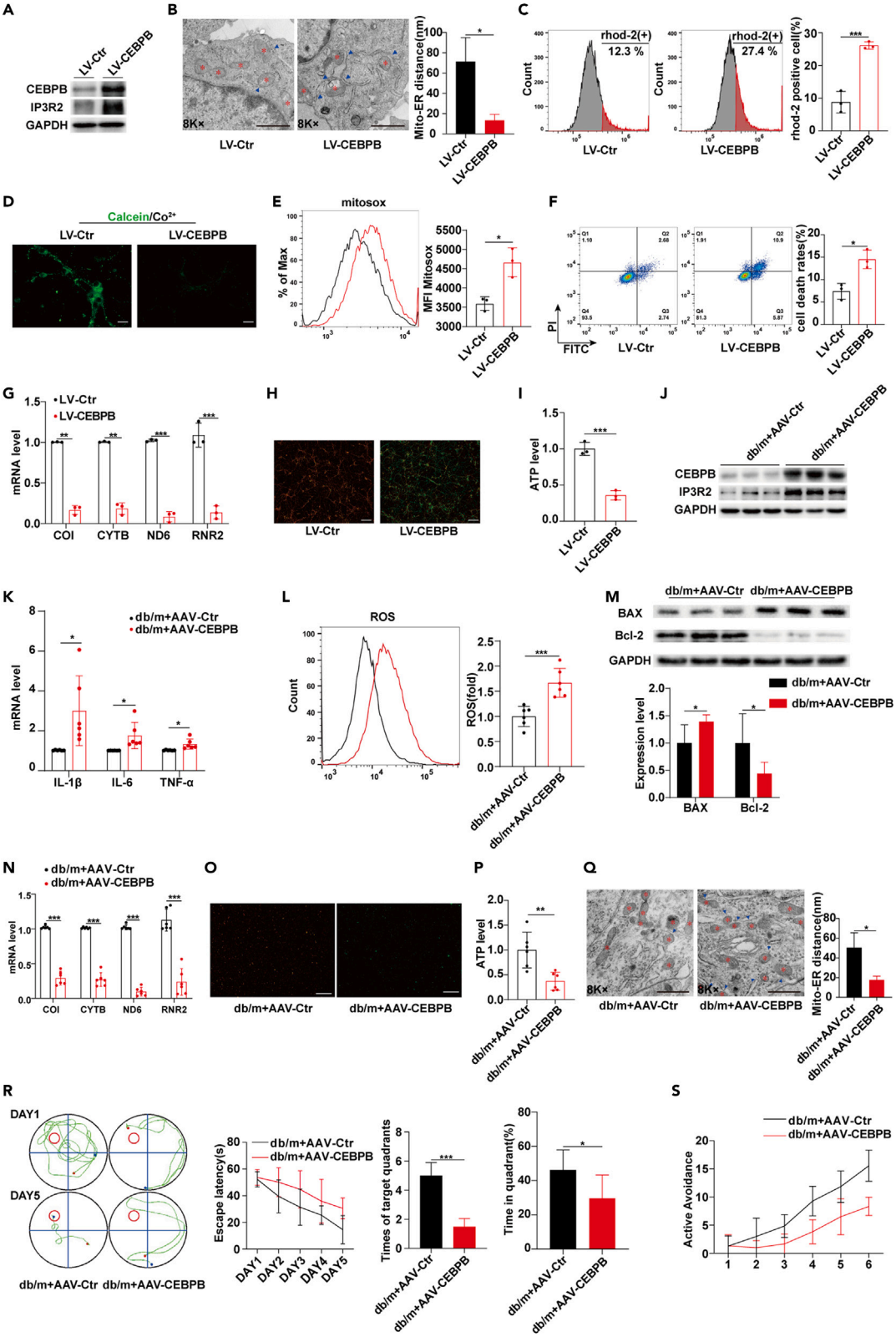
A
LV-Ctr
LV-CEBPB
CEBPB
IP3R2
GAPDH
B
8K×
LV-Ctr
LV-CEBPB
Mito-ER distance(nm)
C
rhod-2(+)
12.3 %
rhod-2(+)
27.4 %
Count
rhod-2 positive cell(%)
D
Calcein/Co²⁺
LV-Ctr
LV-CEBPB
E
mitosox
% of Max
MFI Mitosox
F
PI
FITC
cell death rates(%)
G
LV-Ctr
LV-CEBPB
mRNA level
COI
CYTB
ND6
RNR2
H
LV-Ctr
LV-CEBPB
I
ATP level
J
db/m+AAV-Ctr
db/m+AAV-CEBPB
CEBPB
IP3R2
GAPDH
K
db/m+AAV-Ctr
db/m+AAV-CEBPB
mRNA level
IL-1β
IL-6
TNF-α
L
ROS
Count
ROS(fold)
M
db/m+AAV-Ctr
db/m+AAV-CEBPB
BAX
Bcl-2
GAPDH
Expression level
N
db/m+AAV-Ctr
db/m+AAV-CEBPB
mRNA level
COI
CYTB
ND6
RNR2
O
db/m+AAV-Ctr
db/m+AAV-CEBPB
P
ATP level
Q
8K×
db/m+AAV-Ctr
db/m+AAV-CEBPB
Mito-ER distance(nm)
R
DAY1
DAY5
db/m+AAV-Ctr
db/m+AAV-CEBPB
Escape latency(s)
DAY1
DAY2
DAY3
DAY4
DAY5
Times of target quadrants
Time in quadrant(%)
S
db/m+AAV-Ctr
db/m+AAV-CEBPB
Active Avoidance

Figure 5. Hippocampal overexpression of CEBPB promotes MAM formation, mitochondrial calcium overload, impairs mitochondrial function, and leads to cognitive impairment

(A–I) Immunoblots analysis of protein levels of CEBPB, IP3R2 (A), representative TEM images of the ER and mitochondrial morphology (Scale bar, 1 μm) (B), FCM analysis of mitochondrial calcium levels (C), MPTP opening (D), ROS level (E), apoptosis level (F), mRNA levels of mitochondrial functional genes COI, CYTB, ND6, RNR2 (G), MMP (H), and ATP level (I) in primary hippocampal neurons infected with CEBPB-overexpressing lentivirus or control lentivirus for 72 h.

(J–Q) Immunoblots analysis of protein levels of CEBPB, IP3R2 (J), mRNA levels of inflammatory factors IL-1β, IL-6, TNF-α (K), ROS level (L), immunoblots and quantification analysis of protein levels of BAX and Bcl-2 (M), mRNA levels of mitochondrial functional genes COI, CYTB, ND6, RNR2 (N), MMP (O), ATP level (P), representative TEM images of the ER and mitochondrial morphology (Scale bar, 1 μm) (Q) in the hippocampus of db/m and db/m+ AAV-CEBPB mice. (n = 6/group).

(R) Morris water maze behavioral assessment for db/m and db/m+ AAV-CEBPB mice showing differences in path (left), escape latency (second from left), number of times mice passed through the platform location in the probe trial (second from right) and the time mice stayed in the target quadrant (right) during the learning session. (n = 6/group).

(S) The active avoidance performance of db/m and db/m+ AAV-CEBPB mice. (n = 6/group).

db/m mice (Figures 4J–4Q), confirming the *in vitro* findings that ERp29 promoted MAM formation, mitochondrial calcium overload, and impaired mitochondrial function. In addition, hippocampal overexpression of ERp29 significantly impaired cognitive function in db/m mice (Figures 4R and 4S).

Transcription factor CCAAT/enhancer-binding protein-β promotes the expression of ERp29

To investigate the transcriptional regulation of ERp29 gene expression, a set of ERp29 promoter fragments were inserted into the upstream of the firefly luciferase reporter gene in the pGL3-basic vector and transiently transfected into 293T cells. As shown in Figure S4A, pGL3-801/0 fragments displayed the highest promoter activity among the five fragments. The promoter activity of the pGL3 -252/0 fragments significantly decreased to 56.93% of that of the pGL3 -801/0 fragments, indicating that the −801/0 region was required for the full transcription of ERp29. To investigate further the upstream regulatory mechanism of enhanced ERp29 expression in type 2 diabetes, the region from −801 to −252 was predicted by the online tool ALGGEN to obtain putative transcription factors and their binding sites. Of all these transcription factors, three (CCAAT/enhancer-binding protein-β (CEBPB), JUND, and SP1) putative transcription factors were identified with R values greater than 0.5 (Figure S4B). To investigate their roles in regulating ERp29 gene transcription, these three vectors were respectively, overexpressed in 293T cells transiently transfected with the pGL3-2000/0 construct. CEBPB and SP1 overexpression group significantly increased the promoter activities of pGL3-2000/0 (Figure S4C); however, only CEBPB significantly upregulated ERp29 gene expression (Figure S4D). Three putative CEBPB-binding sites were identified on the ERp29 promoter (Figure S4E). Thus, we introduced three single-site mutations (mut1 (−274 to −261 bp), mut2 (−446 to −440 bp), and mut3 (−523 to −513 bp)) to determine the effects of these three putative CEBPB-binding sites on the promoter activity of ERp29 as assessed by luciferase assay. Mutations in binding sites 1 and 3 significantly decreased ERp29 promoter activity to 60.26 ± 9.13% and 74.25 ± 11.4% respectively in primary hippocampal neurons, whereas mutations in binding sites 2 had no effect on ERp29 promoter activity (Figure S4F). ChIP assays were then conducted to examine whether CEBPB could bind to these two sites. We designed two primer pairs that encompassed the CEBPB-binding sites and qRT-PCR were performed with two primer pairs and ChIP product. As shown in Figure S4G, CEBPB bound directly to the promoter of ERp29 in the range of primer pairs 1 and 2. Collectively, these data suggested that transcription factor CEBPB upregulated the expression of ERp29.

Hippocampal overexpression of CCAAT/enhancer-binding protein-β promotes mitochondria-associated endoplasmic reticulum membrane formation, mitochondrial calcium overload, impairs mitochondrial function, and leads to cognitive impairment

Since CEBPB upregulated ERp29 expression, we next examined the impact of CEBPB overexpression (Figure 5A) on MAM formation, mitochondrial function, and cognitive ability. As illustrated by TEM images (Figure 5B) and flow cytometric analysis (Figure 5C), CEBPB overexpression increased the association between the ER and mitochondria and induced mitochondrial calcium overload in primary hippocampal neurons, these effects were paralleled by an increase in MPTP opening (Figure 5D), ROS generation (Figure 5E), apoptosis (Figure 5F), and a decrease in mitochondria genes expression (Figure 5G), MMP levels (Figure 5H), ATP production (Figure 5I). We further validated these results *in vivo*, consistent with our *in vitro* findings, hippocampal overexpression of CEBPB (Figure 5J) in db/m mice impaired mitochondrial function, revealed by significant increases in inflammatory gene expression (Figure 5K), ROS generation (Figure 5L) and apoptosis (Figure 5M) and significant decreases in mitochondrial genes expressions (Figure 5N), MMP

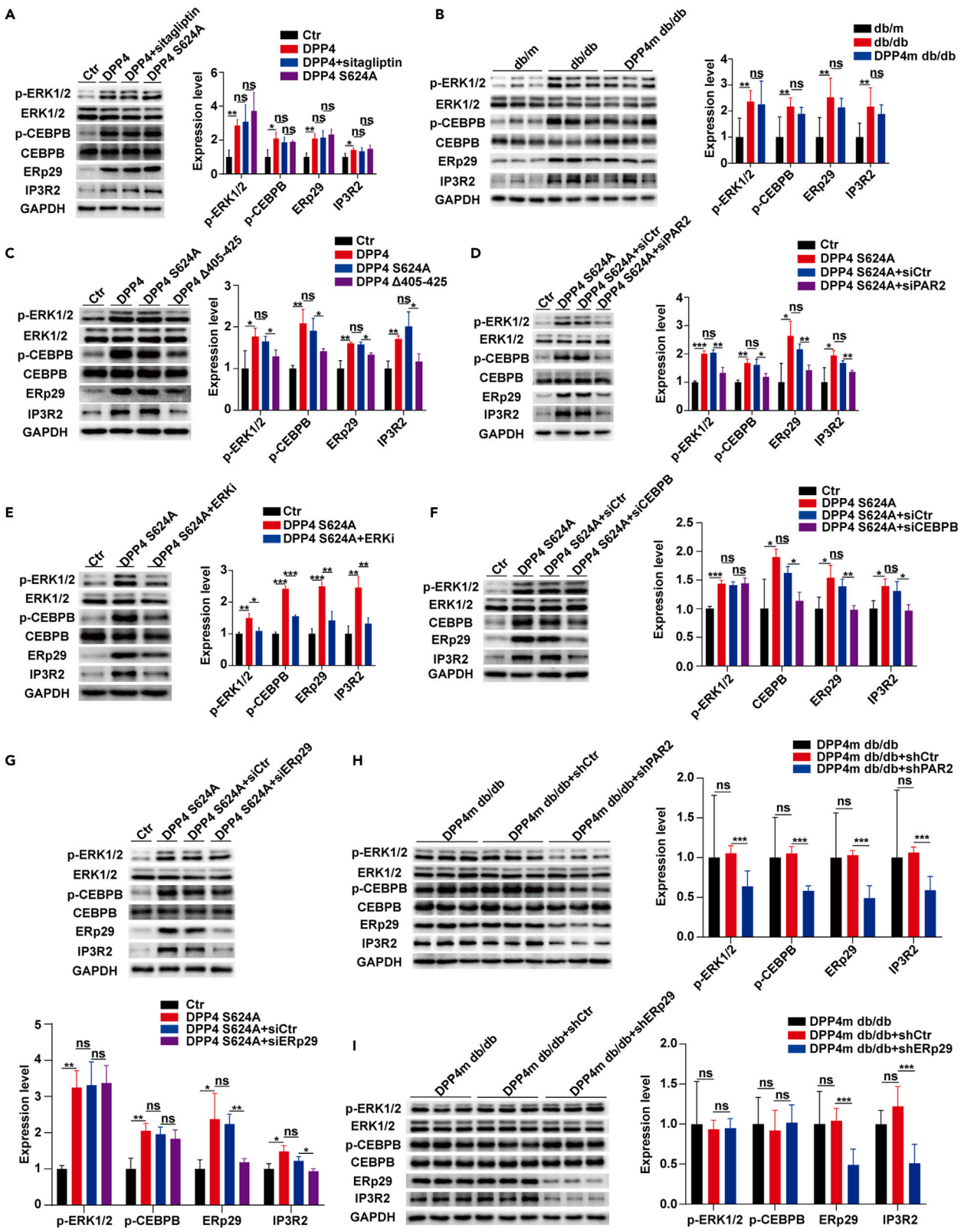
A
Ctr
DPP4
DPP4+sitagliptin
DPP4 S624A
p-ERK1/2
ERK1/2
p-CEBPB
CEBPB
ERp29
IP3R2
GAPDH
Expression level
p-ERK1/2
p-CEBPB
ERp29
IP3R2
B
db/m
db/db
DPP4m db/db
C
DPP4 Δ405-425
D
DPP4 S624A+siCtr
DPP4 S624A+siPAR2
E
DPP4 S624A+ERKi
F
DPP4 S624A+siCEBPB
G
DPP4 S624A+siERp29
H
DPP4m db/db+shCtr
DPP4m db/db+shPAR2
I
DPP4m db/db+shERp29

Figure 6. DPP4 increased Ip3r2 protein expression via PAR2/ERK/CEBPB/ERp29 signaling in an enzymatic activity-independent manner

(A) Immunoblots and quantification analysis of protein levels of *p*-ERK1/2, ERK, *p*-CEBPB, CEBPB, ERp29, and IP3R2 in primary hippocampal neurons treated with DPP4, DPP4+sitagliptin, or DPP4 ^{S624A}, respectively.

(B) Immunoblots and quantification analysis of protein levels of *p*-ERK1/2, ERK, *p*-CEBPB, CEBPB, ERp29, and IP3R2 in the hippocampus from db/m, db/db or DPP4m db/db mice. (n = 6/group).

(C) Immunoblots and quantification analysis of protein levels of *p*-ERK1/2, ERK, *p*-CEBPB, CEBPB, ERp29, and IP3R2 in primary hippocampal neurons treated with DPP4, DPP4 S624A, or DPP4 Δ405-425, respectively.

(D) Immunoblots and quantification analysis of protein levels of *p*-ERK1/2, ERK, *p*-CEBPB, CEBPB, ERp29, and IP3R2 in primary hippocampal neurons treated with DPP4 S624A, DPP4 S624A + siControl or DPP4 S624A + siPAR2, respectively.

(E) Immunoblots and quantification analysis of protein levels of *p*-ERK1/2, ERK, *p*-CEBPB, CEBPB, ERp29, and IP3R2 in primary hippocampal neurons treated with DPP4 S624A or DPP4 S624A + ERKi, respectively.

(F) Immunoblots and quantification analysis of protein levels of *p*-ERK1/2, ERK, CEBPB, ERp29, and IP3R2 in primary hippocampal neurons treated with DPP4 S624A, DPP4 S624A + siControl or DPP4 S624A + siCEBPB, respectively.

(G) Immunoblots and quantification analysis of protein levels of *p*-ERK1/2, ERK, *p*-CEBPB, CEBPB, ERp29, and IP3R2 in primary hippocampal neurons treated with DPP4 S624A, DPP4 S624A + siControl or DPP4 S624A + siERp29, respectively.

(H) Immunoblots and quantification analysis of protein levels of *p*-ERK1/2, ERK, *p*-CEBPB, CEBPB, ERp29, and IP3R2 in the hippocampus from DPP4m db/db, DPP4m db/db+shControl, or DPP4m db/db+shPAR2 mice. (n = 6/group).

(I) Immunoblots and quantification analysis of protein levels of *p*-ERK1/2, ERK, *p*-CEBPB, CEBPB, ERp29, and IP3R2 in the hippocampus from DPP4m db/db, DPP4m db/db+shControl, or DPP4m db/db+shERp29 mice. (n = 6/group).

levels (Figure 5O) and ATP productions (Figure 5P). These changes were accompanied by increased MAM formation (Figure 5Q) and cognitive impairment (Figures 5R and 5S).

DPP4 increased IP3R2 protein expression via PAR2/ERK/CEBPB/ERp29 signaling in an enzymatic activity-independent manner

To explore the potential mechanisms of DPP4-mediated upregulation of IP3R2 expression, we analyzed DPP4-related signaling pathways using the STRING database. Extracellular signal-regulated kinase 1 (ERK)/CEBPB/ERp29 signaling was nominated as a candidate pathway (Figure S5A). DPP4 treatment increased the levels of *p*-ERK1/2, *p*-CEBPB (Phosphorylation levels of CEBPB represented nuclear translocation and transcriptional activation of responsive genes).[27] ERp29 and IP3R2 in primary hippocampal neurons (Figure S5B). Similar to our *in vitro* finding, increased levels of *p*-ERK1/2, *p*-CEBPB, ERp29, and IP3R2 were also detected in the hippocampus of db/db mice and DPP4 knockout significantly decreased the expression of these proteins (Figure S5C).

To investigate whether DPP4-mediated ERK/CEBPB/ERp29 signaling is dependent on its enzymatic activity, we used DPP4 enzymatic inhibitor sitagliptin and catalytically inactive DPP4 mutant by replacing a glycine residue at position 624 with arginine (DPP4 S624A) to inhibit the enzymatic function of DPP4. As shown in Figure 6A, sitagliptin and DPP4 S624A treatment of primary hippocampal neurons did not alter the expression levels of *p*-ERK1/2, *p*-CEBPB, ERp29, and Ip3r2. Similarly, the expression levels of *p*-ERK1/2, *p*-CEBPB, ERp29, and IP3R2 were not significantly changed in DPP4 enzymatic activity mutant db/db mice (DPP4m db/db mice) (Figure 6B), implying that DPP4 might activate ERK/CEBPB/ERp29 signaling via a non-enzymatic pathway. Comparison of DPP4 activity and its protein levels between db/db and DPP4m db/db mice have been presented in Figures S5D and S5E.

Previous studies have shown that soluble DPP4 induces inflammation and microvascular endothelial dysfunction through proteinase-activated receptor-2 (PAR2).[28] To determine whether DPP4 could activate ERK/CEBPB/ERp29 signaling via binding to PAR2, we generated a mutant of DPP4 by truncating amino acids 405-425 (DPP4 Δ405-425), the cysteine-rich region containing the SLIG sequence for PAR2 binding. We found that DPP4 Δ405-425 treatment significantly reduced *p*-ERK1/2, *p*-CEBPB, ERp29, and IP3R2 expression in primary hippocampal neurons (Figure 6C), in addition, DPP4 S624A-induced ERK/CEBPB/ERp29 signaling activation was prevented by PAR2 silencing as well (Figure 6D). Consistent with the above results, rescue experiments further showed that in hippocampal neurons treated with DPP4 S624A, Ip3r2 expression was significantly decreased by ERK inhibitor (Figure 6E), CEBPB silencing (Figure 6F) and ERp29 silencing (Figure 6G). To confirm the *in vitro* findings above, we further tested the effects of hippocampal PAR2 knockdown on ERK/CEBPB/ERp29 signaling in DPP4m db/db mice. As shown in Figure 6H, *p*-ERK1/2, *p*-CEBPB, ERp29, and IP3R2 expression were significantly decreased in the hippocampus of shPAR2-treated db/db mice compared with controls. Similarly, knockdown of

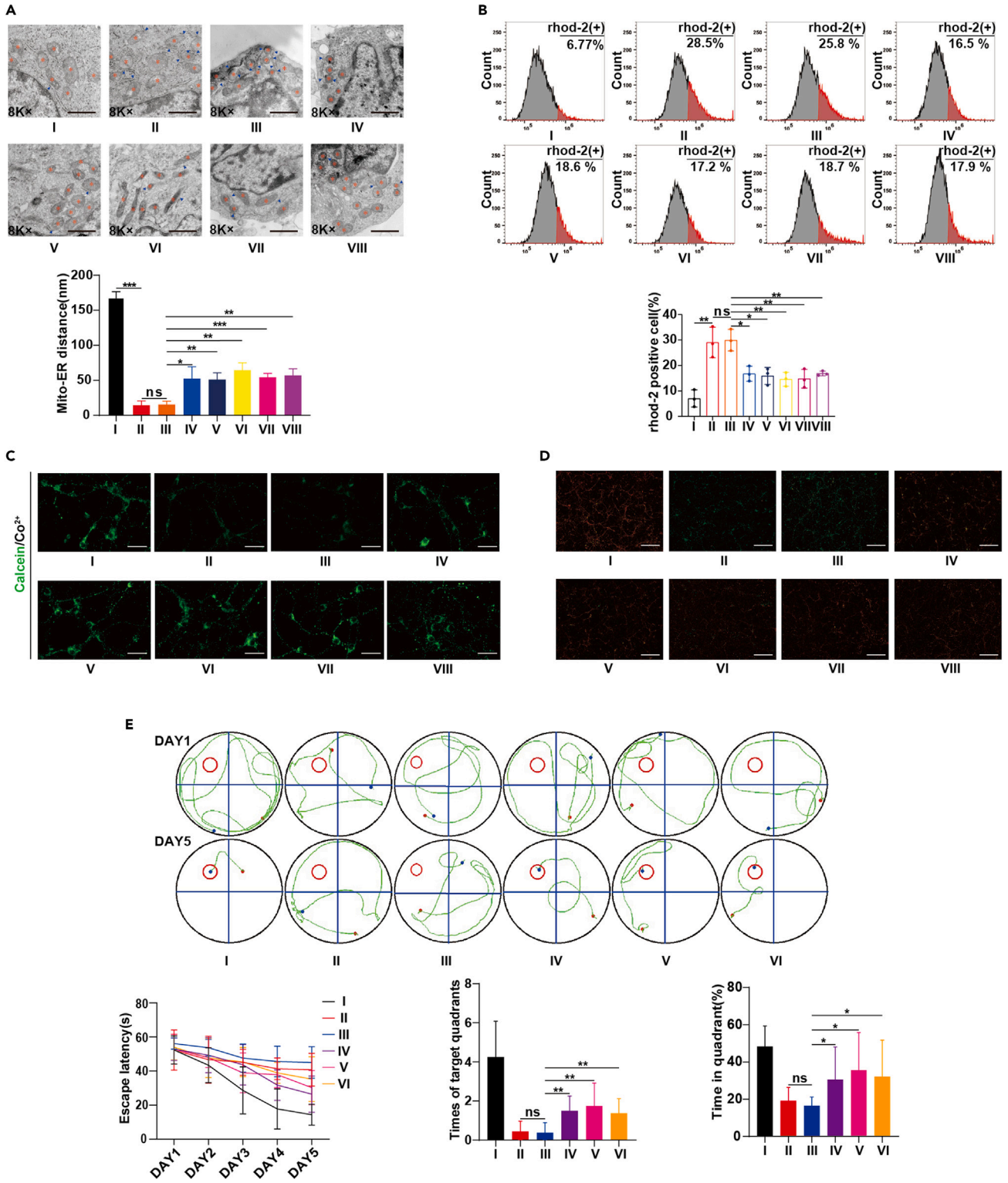

Figure 7. The non-canonical function of DPP4 promotes MAM formation, mitochondrial calcium overload, mitochondrial dysfunction, and cognitive impairment via PAR2/ERK/CEBPB/ERp29 signaling

(A–D) Representative TEM images of the ER and mitochondrial morphology (Scale bar, 1 μm) (A), FCM analysis of mitochondrial calcium levels (B), MPTP opening (C), and MMP (D) in primary hippocampal neurons under different treatments. (Samples: (I) control, (II) DPP4, (III) DPP4 S624A, (IV) DPP4 Δ405-425, (V) DPP4 S624A + PAR2siRNA, (VI) DPP4 S624A + ERKi, (VII) DPP4 S624A + CEBPBsiRNA, (VIII) DPP4 S624A + ERp29siRNA).

Figure 7. *Continued*

(E) Morris water maze behavioral assessment for mice under different treatments. (Samples: (I) db/m, (II) db/db, (III) DPP4m db/db, (IV) DPP4m db/db+shPAR2, (V) DPP4m db/db+shCEBPB, (VI) DPP4m db/db+shERp29) showing differences in path (upper panel), escape latency (bottom left panel), the time mice stayed in the target quadrant (bottom middle panel) and number of times mice passed through the platform location in the probetrial (bottom right panel) during the learning session. (n = 6/group).

both CEBPB (Figure S5F) and ERp29 (Figure 6I) significantly downregulated the expression of IP3R2 in the hippocampus of DPP4m db/db mice. Taken together, these data indicated that DPP4 increased IP3R2 protein expression via PAR2/ERK/CEBPB/ERp29 signaling in an enzymatic activity-independent manner.

The non-canonical function of DPP4 promotes mitochondria-associated endoplasmic reticulum membrane formation, mitochondrial calcium overload, mitochondrial dysfunction, and cognitive impairment via PAR2/ERK/CEBPB/ERp29 signaling

We next examined whether the non-canonical function of DPP4 promotes MAM formation, mitochondrial dysfunction and impairs cognitive ability via PAR2/ERK/CEBPB/ERp29 Signaling. After the treatment of primary hippocampal neurons with DPP4 and DPP4 S624A, MAM formation (Figure 7A), mitochondrial Ca^{2+} levels (Figure 7B), MPTP opening (Figure 7C), ROS generation (Figure S6A) and apoptosis (Figure S6B) were increased, but ATP production (Figure S6C), MMP levels (Figure 7D) and mitochondria genes expression (Figure S6D) were decreased, and these effects were significantly reversed by DPP4 Δ405-425, PAR2 silencing, ERK inhibitor, CEBPB, and ERp29 silencing. Consistent with our *in vitro* findings, db/db and DPP4m db/db mice exhibited an increase in inflammatory gene expression (Figure S6E), ROS generation (Figure S6F), and apoptosis (Figure S6G), and a decrease in mitochondrial genes expressions (Figure S6H), MMP levels (Figure S6I) and ATP productions (Figure S6J) in their hippocampus compared with db/m mice, whereas hippocampal knockdown of PAR2, CEBPB, and ERp29 all significantly reversed these effects and successfully improved cognitive function in DPP4m db/db mice (Figures 7E and S6K). Collectively, our results demonstrated that DPP4 promotes MAM formation, mitochondrial calcium overload, mitochondrial dysfunction, and cognitive impairment via PAR2/ERK/CEBPB/ERp29 signaling in an enzymatic activity-independent manner.

DISCUSSION

In the present study, we demonstrated the important role of DPP4-mediated MAM formation and mitochondrial calcium overload in diabetes-associated cognitive impairment. The key findings of this work are that (1) DPP4-mediated up-regulation of IP3R2 induces MAM formation and mitochondrial calcium overload, which in turn leads to cognitive impairment in diabetes, (2) DPP4 inhibits IP3R2 proteasomal degradation by up-regulating ERp29 expression and promoting its binding to IP3R2, (3) DPP4 promotes MAM formation, mitochondrial calcium overload, and cognitive impairment through PAR2/ERK/CEBPB/ERp29 signaling in an enzymatic activity-independent manner.

A growing number of studies have revealed the importance of the miscommunication between mitochondria and ER in the pathogenesis of cognitive impairment.[6,29] Due to the highly plastic and dynamic nature of MAMs, the spatial-temporal pattern and structural parameters (i.e., the width, length, and number of the MAMs) are important factors in determining the dual and opposing effects of MAM on mitochondrial function. On one hand, moderate and transient increase in MAM ensures the transduction of IP3R-mediated Ca^{2+} signals from ER to mitochondria, which alleviate ER stress, promote mitochondrial biogenesis and improve mitochondrial function. On the other hand, if MAMs couplings are too tight and increase over prolonged period of time, the initially beneficial effects for mitochondrial function would convert to detrimental effects, such as mitochondrial calcium overload, impaired mitochondrial biogenesis and oxidative phosphorylation, and activation of inflammasomes and apoptosis.[25] Consistent with previous studies,[8,30] we found increased contact sites between mitochondria and ER in db/db mice, and the effects of MAMs' dysfunction on cognitive impairment is likely to result from the engagement of multiple pathways, including mitochondrial calcium overload, impaired ATP production, decreased MMP and increased MPTP opening, ROS generation, inflammation, and apoptosis. In addition, we find that IP3R2 is upregulated in the hippocampus of db/db mice and contributes to MAM formation, mitochondrial calcium overload, and cognitive impairment. These results were further confirmed by the overexpression of IP3R2 both *in vitro* and *in vivo*, demonstrating the pathogenetic role of

IP3R2-mediated MAM formation and mitochondrial calcium overload in diabetes-associated cognitive impairment.

ERp29 is a non-classical molecular chaperone of the ER that plays an important role in protein folding, trafficking, and secretion. ERp29 is broadly distributed in neurons and is upregulated in response to ER stress, thus exerting a neuroprotective effect.[26,31] However, our results were inconsistent with these findings. We found that ERp29 is upregulated in the hippocampus of db/db mice and its knockdown significantly reduced MAM formation and alleviate mitochondrial dysfunction and cognitive impairment. Additionally, overexpression of ERp29 induced MAM formation, mitochondrial calcium overload, mitochondrial dysfunction, and cognitive impairment. Moreover, our results demonstrated that the D-domain of ERp9 could bind to IP3R2 and subsequently inhibit its degradation in hippocampal neurons, suggesting a mechanism by which ERp29 induces MAM formation and mitochondrial calcium overload in diabetes-associated cognitive impairment. Previous study by Zou et al. also lent support to our findings, their results demonstrated that ERp29 inhibition significantly reversed taurocholic acid toxicity via attenuating G2/M arrest and cell apoptosis.[32] The reason for this discrepancy may be attributed to the possible dual role of ERp29 in regulating mitochondrial function under ER stress conditions such as diabetes. We speculate that ERp29 might play a protective role in the early stage of ER stress through enhanced IP3R2-mediated ER-mitochondrial Ca^{2+} transport and mitochondrial biogenesis, once these stress conditions become persistent and progressive, the protective mechanism might become detrimental to mitochondrial function and cell survival due to increased IP3R2-mediated MAM formation and mitochondrial calcium overload. It remains to be determined whether ERp29-mediated calcium overload could also play a role in other tissues and disease pathologies in addition to its effects on neuronal cells in diabetes.

ERK1 and ERK2 are the downstream components of a phosphorelay pathway that transduces growth, metabolic and mitogenic signals mediated by the small RAS GTPases. By phosphorylating a series of substrates, ERK signaling plays a crucial role in a variety of cellular processes, such as cell proliferation, growth, metabolism, differentiation, and development. There is increasing evidence suggesting that the dysregulation of ERK signaling contributes to a wide spectrum of human diseases, including metabolic disorders, neurodegeneration, aging, and cancer.[33] The detrimental effects of ERK1/2 signaling in diabetes are manifested as oxidative stress and apoptosis,[34,35] in addition, ERK1/2 signaling has been proved to phosphorylate transcription factor CEBPB and promote its nuclear localization to activate the transcription of a wide range of genes.[36–38] In this study, we found a significant activation of ERK1/2 signaling in the hippocampus of db/db mice, which further upregulated the expression of ERp29 via phosphorylation and nuclear localization of CEBPB. Moreover, CEBPB overexpression in hippocampal neurons produced a phenotype similar to that induced by overexpression of ERp29 and IP3R2, including increased MAM formation, mitochondrial calcium overload, mitochondrial dysfunction, and cognitive impairment. Our finding is consistent with previous reports that demonstrate the pathogenetic role of CEBPB in neurotoxicity and Alzheimer's disease.[39,40] Together, we validated the ERK1/2 signaling-mediated upregulation of ERp29 by CEBPB in diabetes-associated cognitive impairment.

DPP4 has been proven to exert its functions by both enzymatic and non-enzymatic pathways.[5] Our previous research has demonstrated the non-enzymatic role of DPP4 in diabetes-associated mitochondrial dysfunction and cognitive impairment via targeting PAR2/GSK-3β/PGC-1α signaling pathway. In the present study, we provide further insight into the possible mechanism by which DPP4 induces MAM formation and mitochondrial calcium overload in hippocampal neurons, both *in vivo* and *in vitro* experiments demonstrated that DPP4 bound to PAR2 in hippocampal neurons and activate ERK1/2/CEBPB signaling, which upregulates ERp29 expression and leads to MAM formation and mitochondrial calcium overload, thereby promoting cognitive impairment in type 2 diabetes. Notably, DPP4 significantly altered the morphology of neuronal mitochondria, characterized by swollen mitochondria with disorganized cristae. In addition, our previous finding reported that DPP4 downregulated the expression of mitochondrial transcription factor A and mitofusin-1 in neuronal mitochondria.[5] These results suggested that DPP4-induced morphology change might be correlated with impaired mitochondrial dynamics and quality control in hippocampal neurons. Previous studies have revealed an interaction between DPP4 and PAR2 in regulating fibroblast activation,[41] endothelial function,[28,42] and adipose inflammation and insulin resistance,[43] strongly suggesting that DPP4 could exert pleiotropic effects via different signaling pathways in an enzymatic activity-independent manner. The non-canonical role of DPP4 in MAM formation and mitochondrial calcium overload we presented here may partly explain why DPP4 enzymatic inhibitors do not improve cognitive function in type 2 diabetes.[20] The reason why peripheral DPP4 could exert a deleterious effect on hippocampal neurons is considered as follows: DPP4 is widely expressed on different subsets of T cells in the

peripheral circulation, impaired blood-brain barrier integrity under high glucose conditions might lead to increased T cells infiltration into the brain, resulting in enhanced expression of DPP4 in the hippocampus,[5] whether DPP4 could cross the blood-brain barrier by itself warrants further investigation.

In conclusion, this study reveals that ERK1/2/CEBPB signaling facilitates the DPP4-mediated upregulation of ERp29, which subsequently inhibits the degradation of IP3R2 in MAM and finally promotes mitochondrial calcium overload and cognitive impairment in type 2 diabetes. Our study reveals the non-canonical role of DPP4 in regulating MAM formation and mitochondrial calcium overload and identifies DPP4-mediated PAR2/ERK1/2/CEBPB/ERp29 signaling as a promising therapeutic target for the treatment of cognitive impairment in type 2 diabetes.

Limitations of the study

The lack of autopsy data is the first limitation of this study as postmortem analysis would be helpful to further elucidate the precise function of DPP4-mediated PAR2/ERK1/2/CEBPB/ERp29 signaling in type 2 diabetes. Second, the detailed mechanisms underlying ERK1/2 activation by interaction between DPP4 and PAR2 have not been determined. Third, although non-enzymatic effects of DPP4 have been clearly demonstrated in cultured hippocampal neuron cells, *in vivo* analysis using DPP4 conventional knockout mice does not rule out the possibility that some effects are mediated by other cells than hippocampal neuron, such as microglia and immune cells. Further investigation is required to clarify the effects of DPP4 on microglia and immune cells. Fourth, previous study has reported that IP3R has three isoforms and neurons tend to have high expression levels of IP3R1.[44] IP3R1 and IP3R2 share ~70% amino acid sequence homology and the same key functional domains.[45] In this study, we found that IP3R1 expression in MAM was also upregulated after DPP4 treatment. However, it remains unclear whether this effect could be attributed to DPP4-mediated upregulation of ERp29. Fifth, in this study, we used a published dataset to analyze the proteome changes in MAM under diabetic conditions and identified ERp29 as a possible target of DPP4. This way of investigation might introduce some bias since the direct effect of DPP4 on ERp29 expression cannot be confirmed in this proteomic analysis. In addition to ERp29, there may also exist other pathways by which DDP4 could regulate the protein level of IP3R2. Sixth, it is generally acknowledged that mitochondrial calcium homeostasis is maintained in a coordinated fashion by regulators controlling calcium influx and efflux,[30] how DPP4 regulates mitochondrial calcium efflux in hippocampal neurons warrants further investigation. Seventh, planimetric analysis alone might not be able to precisely measure the distance between ER and mitochondria because of the stereostructure of MAM, *in situ* proximity ligation assay experiments or 3D image analysis could be helpful for future research. Finally, all interventions targeting DPP4-mediated PAR2/ERK1/2/CEBPB/ERp29 signaling were conducted by hippocampal injection, gene mutation, or knockout animal models, further studies are needed to develop oral drug delivery systems to penetrate the blood-brain barrier and target the PAR2/ERK1/2/CEBPB/ERp29 signaling pathway.

STAR★METHODS

Detailed methods are provided in the online version of this paper and include the following:

- KEY RESOURCES TABLE
- RESOURCE AVAILABILITY
  - Lead contact
  - Materials availability
  - Data and code availability
- EXPERIMENTAL MODEL AND SUBJECT DETAILS
  - Ethical approval
  - Mice
  - Cell isolation and culture
- METHOD DETAILS
  - Stereotaxic injection
  - Gene silencing and overexpression
  - Isolation of MAM
  - Immunoprecipitation and immunoblot analysis
  - RNA extraction and RT-qPCR
  - Immunofluorescence
  - Chromatin immunoprecipitation

- Mitochondrial membrane potential assay
- ATP measurement
- Detection of reactive oxygen species (ROS)
- Apoptosis analysis
- Mitochondrial Ca^{2+} measurement
- Transmission electron microscopy (TEM)
- TUNEL staining
- MPTP
- Luciferase assays
- Morris water maze
- Active avoidance memory test
- DPP4 enzyme activity
- Bioinformatics analysis

● QUANTIFICATION AND STATISTICAL ANALYSIS

SUPPLEMENTAL INFORMATION

Supplemental information can be found online at https://doi.org/10.1016/j.isci.2023.106271.

ACKNOWLEDGMENTS

We kindly thank Haifan Zou and Weiyuan Liang from Science and Research Center at Guilin Medical University for their technical assistance with electron microscopy. This study was supported by grants from the National Natural Science Foundation of China (Grant No. 82260171, 81770829, and 81560144), the Natural Science Foundation of Guangxi Province for Distinguished Young Scholars (Grant No. 2021GXNSFFA196003), the Scientific Research and Technology Development Projects of Science and Technology Department of Guangxi Province (Grant No. 1598012-13), the Natural Science Foundation of Guangxi Province (Grant No. 2015GXNSFBA139119 and 2018GXNSFAA281359), the High-Level Medical Talents Training Program of Guangxi Province (G201903002), the Innovation Project of Guangxi Graduate Education (No.YCSW2022378) and the Graduate Research Program of Guilin Medical University (No.GYYK2022016).

AUTHOR CONTRIBUTIONS

T.P.Z. supervised the study and designed the experiments. J.X.L., Y.H., Z.Q.X., L.Y.K., Y.Y.T., J.J.W. and Q.S.Z. performed experiments and analyzed results. T.P.Z. wrote the article. J.T. and K.Y. reviewed the article.

DECLARATION OF INTERESTS

The authors declare no competing interests.

INCLUSION AND DIVERSITY

We support inclusion, diverse, and equitable conduct of research.

Received: July 22, 2022
Revised: January 15, 2023
Accepted: February 19, 2023
Published: February 27, 2023

REFERENCES

1. van Sloten, T.T., Sedaghat, S., Carnethon, M.R., Launer, L.J., and Stehouwer, C.D.A. (2020). Cerebral microvascular complications of type 2 diabetes: stroke, cognitive dysfunction, and depression. Lancet Diabetes Endocrinol. *8*, 325–336. https://doi.org/10.1016/S2213-8587(19)30405-X.

2. Roberts, R.O., Knopman, D.S., Geda, Y.E., Cha, R.H., Pankratz, V.S., Baertlein, L., Boeve, B.F., Tangalos, E.G., Ivnik, R.J., Mielke, M.M., and Petersen, R.C. (2014). Association of diabetes with amnestic and nonamnestic mild cognitive impairment. Alzheimers Dement. *10*, 18–26. https://doi.org/10.1016/j.jalz.2013.01.001.

3. Fernandez, A., Meechan, D.W., Karpinski, B.A., Paronett, E.M., Bryan, C.A., Rutz, H.L., Radin, E.A., Lubin, N., Bonner, E.R., Popratiloff, A., et al. (2019). Mitochondrial dysfunction leads to cortical under-connectivity and cognitive impairment. Neuron *102*, 1127–1142.e3. https://doi.org/10.1016/j.neuron.2019.04.013.

4. Song, T., Song, X., Zhu, C., Patrick, R., Skurla, M., Santangelo, I., Green, M., Harper, D., Ren, B., Forester, B.P., et al. (2021). Mitochondrial dysfunction, oxidative stress,

neuroinflammation, and metabolic alterations in the progression of Alzheimer's disease: a meta-analysis of in vivo magnetic resonance spectroscopy studies. Ageing Res. Rev. *72*, 101503. https://doi.org/10.1016/j.arr.2021.101503.

5. Sun, C., Xiao, Y., Li, J., Ge, B., Chen, X., Liu, H., and Zheng, T. (2022). Nonenzymatic function of DPP4 in diabetes-associated mitochondrial dysfunction and cognitive impairment. Alzheimers Dement. *18*, 966–987. https://doi.org/10.1002/alz.12437.

6. Paillusson, S., Stoica, R., Gomez-Suaga, P., Lau, D.H.W., Mueller, S., Miller, T., and Miller, C.C.J. (2016). There's something wrong with my MAM; the ER-mitochondria axis and neurodegenerative diseases. Trends Neurosci. *39*, 146–157. https://doi.org/10.1016/j.tins.2016.01.008.

7. Filipe, A., Chernorudskiy, A., Arbogast, S., Varone, E., Villar-Quiles, R.N., Pozzer, D., Moulin, M., Fumagalli, S., Cabet, E., Dudhal, S., et al. (2021). Defective endoplasmic reticulum-mitochondria contacts and bioenergetics in SEPN1-related myopathy. Cell Death Differ. *28*, 123–138. https://doi.org/10.1038/s41418-020-0587-z.

8. Lee, H.J., Jung, Y.H., Choi, G.E., Kim, J.S., Chae, C.W., Lim, J.R., Kim, S.Y., Yoon, J.H., Cho, J.H., Lee, S.J., and Han, H.J. (2021). Urolithin A suppresses high glucose-induced neuronal amyloidogenesis by modulating TGM2-dependent ER-mitochondria contacts and calcium homeostasis. Cell Death Differ. *28*, 184–202. https://doi.org/10.1038/s41418-020-0593-1.

9. Wu, S., Lu, Q., Ding, Y., Wu, Y., Qiu, Y., Wang, P., Mao, X., Huang, K., Xie, Z., and Zou, M.H. (2019). Hyperglycemia-driven inhibition of AMP-activated protein kinase alpha2 induces diabetic cardiomyopathy by promoting mitochondria-associated endoplasmic reticulum membranes in vivo. Circulation *139*, 1913–1936. https://doi.org/10.1161/CIRCULATIONAHA.118.033552.

10. Wang, C., Dai, X., Wu, S., Xu, W., Song, P., and Huang, K. (2021). FUNDC1-dependent mitochondria-associated endoplasmic reticulum membranes are involved in angiogenesis and neoangiogenesis. Nat. Commun. *12*, 2616. https://doi.org/10.1038/s41467-021-22771-3.

11. Yang, S., Harding, A.T., Sweeney, C., Miao, D., Swan, G., Zhou, C., Jiang, Z., Fitzgerald, K.A., Hammer, G., Bergo, M.O., et al. (2019). Control of antiviral innate immune response by protein geranylgeranylation. Sci. Adv. *5*, eaav7999. https://doi.org/10.1126/sciadv.aav7999.

12. Field, C.S., Baixauli, F., Kyle, R.L., Puleston, D.J., Cameron, A.M., Sanin, D.E., Hippen, K.L., Loschi, M., Thangavelu, G., Corrado, M., et al. (2020). Mitochondrial integrity regulated by lipid metabolism is a cell-intrinsic checkpoint for treg suppressive function. Cell Metabol. *31*, 422–437.e5. https://doi.org/10.1016/j.cmet.2019.11.021.

13. Hu, M., Zhou, M., Bao, X., Pan, D., Jiao, M., Liu, X., Li, F., and Li, C.Y. (2021). ATM inhibition enhances cancer immunotherapy by promoting mtDNA leakage and cGAS/STING activation. J. Clin. Invest. *131*, e139333. https://doi.org/10.1172/JCI139333.

14. Baggio, L.L., Varin, E.M., Koehler, J.A., Cao, X., Lokhnygina, Y., Stevens, S.R., Holman, R.R., and Drucker, D.J. (2020). Plasma levels of DPP4 activity and sDPP4 are dissociated from inflammation in mice and humans. Nat. Commun. *11*, 3766. https://doi.org/10.1038/s41467-020-17556-z.

15. Varin, E.M., Mulvihill, E.E., Beaudry, J.L., Pujadas, G., Fuchs, S., Tanti, J.F., Fazio, S., Kaur, K., Cao, X., Baggio, L.L., et al. (2019). Circulating levels of soluble dipeptidyl peptidase-4 are dissociated from inflammation and induced by enzymatic DPP4 inhibition. Cell Metabol. *29*, 320–334.e5. https://doi.org/10.1016/j.cmet.2018.10.001.

16. Zhong, J., Maiseyeu, A., Davis, S.N., and Rajagopalan, S. (2015). DPP4 in cardiometabolic disease: recent insights from the laboratory and clinical trials of DPP4 inhibition. Circ. Res. *116*, 1491–1504. https://doi.org/10.1161/CIRCRESAHA.116.305665.

17. Zheng, T., Liu, H., Qin, L., Chen, B., Zhang, X., Hu, X., Xiao, L., and Qin, S. (2018). Oxidative stress-mediated influence of plasma DPP4 activity to BDNF ratio on mild cognitive impairment in elderly type 2 diabetic patients: results from the GDMD study in China. Metabolism *87*, 105–112. https://doi.org/10.1016/j.metabol.2018.03.014.

18. Wu, C.Y., Ouk, M., Wong, Y.Y., Anita, N.Z., Edwards, J.D., Yang, P., Shah, B.R., Herrmann, N., Lanctôt, K.L., Kapral, M.K., et al. (2020). Relationships between memory decline and the use of metformin or DPP4 inhibitors in people with type 2 diabetes with normal cognition or Alzheimer's disease, and the role APOE carrier status. Alzheimers Dement. *16*, 1663–1673. https://doi.org/10.1002/alz.12161.

19. Isik, A.T., Soysal, P., Yay, A., and Usarel, C. (2017). The effects of sitagliptin, a DPP-4 inhibitor, on cognitive functions in elderly diabetic patients with or without Alzheimer's disease. Diabetes Res. Clin. Pract. *123*, 192–198. https://doi.org/10.1016/j.diabres.2016.12.010.

20. Biessels, G.J., Verhagen, C., Janssen, J., van den Berg, E., Zinman, B., Rosenstock, J., George, J.T., Passera, A., Schnaidt, S., and Johansen, O.E.; CARMELINA Investigators (2019). Effect of linagliptin on cognitive performance in patients with type 2 diabetes and cardiorenal comorbidities: the CARMELINA randomized trial. Diabetes Care *42*, 1930–1938. https://doi.org/10.2337/dc19-0783.

21. Arruda, A.P., and Hotamisligil, G.S. (2015). Calcium homeostasis and organelle function in the pathogenesis of obesity and diabetes. Cell Metabol. *22*, 381–397. https://doi.org/10.1016/j.cmet.2015.06.010.

22. Lopez-Manzaneda, M., Franco-Espin, J., Tejero, R., Cano, R., and Tabares, L. (2021). Calcium is reduced in presynaptic mitochondria of motor nerve terminals during neurotransmission in SMA mice. Hum. Mol. Genet. *30*, 629–643. https://doi.org/10.1093/hmg/ddab065.

23. Ma, J.H., Shen, S., Wang, J.J., He, Z., Poon, A., Li, J., Qu, J., and Zhang, S.X. (2017). Comparative proteomic analysis of the mitochondria-associated ER membrane (MAM) in a long-term type 2 diabetic rodent model. Sci. Rep. *7*, 2062. https://doi.org/10.1038/s41598-017-02213-1.

24. Liu, Z.J., Zhao, W., Lei, H.Y., Xu, H.L., Lai, L.Y., Xu, R., and Xu, S.Y. (2019). High glucose enhances bupivacaine-induced neurotoxicity via MCU-mediated oxidative stress in SH-SY5Y cells. Oxid. Med. Cell. Longev. *2019*, 7192798. https://doi.org/10.1155/2019/7192798.

25. Gao, P., Yang, W., and Sun, L. (2020). Mitochondria-associated endoplasmic reticulum membranes (MAMs) and their prospective roles in kidney disease. Oxid. Med. Cell. Longev. *2020*, 3120539. https://doi.org/10.1155/2020/3120539.

26. Brecker, M., Khakhina, S., Schubert, T.J., Thompson, Z., and Rubenstein, R.C. (2020). The probable, possible, and novel functions of ERp29. Front. Physiol. *11*, 574339. https://doi.org/10.3389/fphys.2020.574339.

27. Oikonomou, V., Moretti, S., Renga, G., Galosi, C., Borghi, M., Pariano, M., Puccetti, M., Palmerini, C.A., Amico, L., Carotti, A., et al. (2016). Noncanonical fungal autophagy inhibits inflammation in response to IFN-gamma via DAPK1. Cell Host Microbe *20*, 744–757. https://doi.org/10.1016/j.chom.2016.10.012.

28. Wronkowitz, N., Görgens, S.W., Romacho, T., Villalobos, L.A., Sánchez-Ferrer, C.F., Peiró, C., Sell, H., and Eckel, J. (2014). Soluble DPP4 induces inflammation and proliferation of human smooth muscle cells via protease-activated receptor 2. Biochim. Biophys. Acta *1842*, 1613–1621. https://doi.org/10.1016/j.bbadis.2014.06.004.

29. Gil-Hernández, A., and Silva-Palacios, A. (2020). Relevance of endoplasmic reticulum and mitochondria interactions in age-associated diseases. Ageing Res. Rev. *64*, 101193. https://doi.org/10.1016/j.arr.2020.101193.

30. Yu, W., Jin, H., and Huang, Y. (2021). Mitochondria-associated membranes (MAMs): a potential therapeutic target for treating Alzheimer's disease. Clin. Sci. *135*, 109–126. https://doi.org/10.1042/CS20200844.

31. McLaughlin, T., Falkowski, M., Wang, J.J., and Zhang, S.X. (2018). Molecular chaperone ERp29: a potential target for cellular protection in retinal and neurodegenerative diseases. Adv. Exp. Med. Biol. *1074*, 421–427. https://doi.org/10.1007/978-3-319-75402-4_52.

32. Zou, S., Zou, P., Wang, Y., Dong, R., Wang, J., Li, N., Wang, T., Zhou, T., Chen, Z., Zhang, Y., et al. (2019). ERp29 inhibition attenuates TCA toxicity via affecting p38/p53- dependent pathway in human trophoblast HTR-8/SVeno cells. Arch. Biochem. Biophys. *676*, 108125. https://doi.org/10.1016/j.abb.2019.108125.

33. Lavoie, H., Gagnon, J., and Therrien, M. (2020). ERK signalling: a master regulator of cell behaviour, life and fate. Nat. Rev. Mol. Cell Biol. *21*, 607–632. https://doi.org/10.1038/s41580-020-0255-7.

34. Maedler, K., Størling, J., Sturis, J., Zuellig, R.A., Spinas, G.A., Arkhammar, P.O.G., Mandrup-Poulsen, T., and Donath, M.Y. (2004). Glucose- and interleukin-1beta-induced beta-cell apoptosis requires Ca2+ influx and extracellular signal-regulated kinase (ERK) 1/2 activation and is prevented by a sulfonylurea receptor 1/inwardly rectifying K+ channel 6.2 (SUR/Kir6.2) selective potassium channel opener in human islets. Diabetes *53*, 1706–1713. https://doi.org/10.2337/diabetes.53.7.1706.

35. Tian, J., Zhao, Y., Liu, Y., Liu, Y., Chen, K., and Lyu, S. (2017). Roles and mechanisms of herbal medicine for diabetic cardiomyopathy: current status and perspective. Oxid. Med. Cell. Longev. *2017*, 8214541. https://doi.org/10.1155/2017/8214541.

36. Roy, S.K., Hu, J., Meng, Q., Xia, Y., Shapiro, P.S., Reddy, S.P.M., Platanias, L.C., Lindner, D.J., Johnson, P.F., Pritchard, C., et al. (2002). MEKK1 plays a critical role in activating the transcription factor C/EBP-beta-dependent gene expression in response to IFN-gamma. Proc. Natl. Acad. Sci. USA *99*, 7945–7950. https://doi.org/10.1073/pnas.122075799.

37. Gade, P., Roy, S.K., Li, H., Nallar, S.C., and Kalvakolanu, D.V. (2008). Critical role for transcription factor C/EBP-beta in regulating the expression of death-associated protein kinase 1. Mol. Cell Biol. *28*, 2528–2548. https://doi.org/10.1128/MCB.00784-07.

38. Harris, V.K., Kagan, B.L., Ray, R., Coticchia, C.M., Liaudet-Coopman, E.D., Wellstein, A., and Tate Riegel, A. (2001). Serum induction of the fibroblast growth factor-binding protein (FGF-BP) is mediated through ERK and p38 MAP kinase activation and C/EBP-regulated transcription. Oncogene *20*, 1730–1738. https://doi.org/10.1038/sj.onc.1204249.

39. Yao, Y., Kang, S.S., Xia, Y., Wang, Z.H., Liu, X., Muller, T., Sun, Y.E., and Ye, K. (2021). A delta-secretase-truncated APP fragment activates CEBPB, mediating Alzheimer's disease pathologies. Brain *144*, 1833–1852. https://doi.org/10.1093/brain/awab062.

40. Ndoja, A., Reja, R., Lee, S.H., Webster, J.D., Ngu, H., Rose, C.M., Kirkpatrick, D.S., Modrusan, Z., Chen, Y.J.J., Dugger, D.L., et al. (2020). Ubiquitin ligase COP1 suppresses neuroinflammation by degrading c/EBPbeta in microglia. Cell *182*, 1156–1169.e12. https://doi.org/10.1016/j.cell.2020.07.011.

41. Lee, S.Y., Wu, S.T., Liang, Y.J., Su, M.J., Huang, C.W., Jao, Y.H., and Ku, H.C. (2020). Soluble dipeptidyl peptidase-4 induces fibroblast activation through proteinase-activated receptor-2. Front. Pharmacol. *11*, 552818. https://doi.org/10.3389/fphar.2020.552818.

42. Romacho, T., Vallejo, S., Villalobos, L.A., Wronkowitz, N., Indrakusuma, I., Sell, H., Eckel, J., Sánchez-Ferrer, C.F., and Peiró, C. (2016). Soluble dipeptidyl peptidase-4 induces microvascular endothelial dysfunction through proteinase-activated receptor-2 and thromboxane A2 release. J. Hypertens. *34*, 869–876. https://doi.org/10.1097/HJH.0000000000000886.

43. Ghorpade, D.S., Ozcan, L., Zheng, Z., Nicoloro, S.M., Shen, Y., Chen, E., Blüher, M., Czech, M.P., and Tabas, I. (2018). Hepatocyte-secreted DPP4 in obesity promotes adipose inflammation and insulin resistance. Nature *555*, 673–677. https://doi.org/10.1038/nature26138.

44. Bannai, H., Niwa, F., Sherwood, M.W., Shrivastava, A.N., Arizono, M., Miyamoto, A., Sugiura, K., Lévi, S., Triller, A., and Mikoshiba, K. (2015). Bidirectional control of synaptic GABAAR clustering by glutamate and calcium. Cell Rep. *13*, 2768–2780. https://doi.org/10.1016/j.celrep.2015.12.002.

45. Prole, D.L., and Taylor, C.W. (2019). Structure and function of IP(3) receptors. Cold Spring Harbor Perspect. Biol. *11*, a035063. https://doi.org/10.1101/cshperspect.a035063.

46. Zhao, Y., Hu, D., Wang, R., Sun, X., Ropelewski, P., Hubler, Z., Lundberg, K., Wang, Q., Adams, D.J., Xu, R., and Qi, X. (2022). ATAD3A oligomerization promotes neuropathology and cognitive deficits in Alzheimer's disease models. Nat. Commun. *13*, 1121. https://doi.org/10.1038/s41467-022-28769-9.

STAR★METHODS

KEY RESOURCES TABLE

REAGENT or RESOURCE	SOURCE	IDENTIFIER
Antibodies		
Rabbit polyclonal anti-PAR2	Abcam	Cat#ab124227; RRID:AB_10975641
Rabbit polyclonal anti-CD26	Thermo Fisher Scientific	Cat#PA1-8455; RRID:AB_2093572
Mouse monoclonal anti-CD26	Santa Cruz Biotechnology	Cat#sc-52642; RRID:AB_629016
Rabbit monoclonal anti-Phospho-p44/42 MAPK (Erk1/2)	Cell Signaling Technology	Cat#4370S; RRID:AB_2315112
Rabbit monoclonal anti-p44/42 MAPK (Erk1/2)	Cell Signaling Technology	Cat#4695S; RRID:AB_390779
Mouse monoclonal anti-C/EBPβ	Santa Cruz Biotechnology	Cat#sc-7962; RRID: AB_626772
Rabbit monoclonal anti-Phospho-C/EBPβ (Thr235)	Cell Signaling Technology	Cat#3084S; RRID: AB_2260359
Rabbit polyclonal anti-ERp29	Proteintech	Cat#24344-1-AP; RRID:AB_2879503
Mouse monoclonal anti-IP3R-II	Santa Cruz Biotechnology	Cat#sc-398434; RRID:AB_2637028
Mouse monoclonal anti-IP3R-I	Santa Cruz Biotechnology	Cat#sc-271197; RRID:AB_10610775
Rabbit polyclonal anti-VDAC1	Proteintech	Cat#55259-1-AP; RRID:AB_10837225
Rabbit polyclonal anti-GAPDH	Proteintech	Cat#10494-1-AP; RRID:AB_2263076
Rabbit polyclonal anti-Calreticulin	Proteintech	Cat#10292-1-AP; RRID:AB_513777
Rabbit polyclonal anti-FACL4	Proteintech	Cat#22401-1-AP; RRID:AB_2832995
Rabbit polyclonal anti-Cytochrome C	Proteintech	Cat#10993-1-AP; RRID:AB_2090467
Rabbit polyclonal anti-Tubulin	Proteintech	Cat#10068-1-AP; RRID:AB_2303998
Rabbit polyclonal anti-BAX	Proteintech	Cat#50599-2-Ig; RRID:AB_2061561
Rabbit polyclonal anti-Bcl-2	Proteintech	Cat#26593-1-AP; RRID:AB_2818996
Goat anti-mouse IgG	Proteintech	Cat#SA00001-1; RRID:AB_2722565
Goat anti-rabbit IgG	Proteintech	Cat#SA00001-2; RRID:AB_2722564
CoraLite488 – conjugated Affinipure Goat Anti-Rabbit	Proteintech	Cat#SA00013-2; RRID: AB_2797132
CoraLite488 – conjugated Affinipure Goat Anti- mouse	Proteintech	Cat#SA00013-1; RRID:AB_2810983
CoraLite594 – conjugated Affinipure Goat Anti-Rabbit	Proteintech	Cat#SA00013-4; RRID:AB_2810984
CoraLite594 – conjugated Affinipure Goat Anti- mouse	Proteintech	Cat#SA00013-3; RRID:AB_2797133
Bacterial and virus strains		
rAAV-shRNA2(IP3R2)	This paper	N/A
rAAV-shRNA2(ERp29)	This paper	N/A
rAAV-shRNA2(CEBPB)	This paper	N/A
rAAV-shRNA2(PAR2)	This paper	N/A
rAAV-shRNA2(scramble)	This paper	N/A
rAAV-IP3R2	This paper	N/A
rAAV-ERp29	This paper	N/A
rAAV-CEBPB	This paper	N/A
rAAV-CON	This paper	N/A
LV-ERp29	This paper	N/A
LV-CEBPB	This paper	N/A
LV-IP3R2	This paper	N/A

(*Continued on next page*)

Continued

REAGENT or RESOURCE	SOURCE	IDENTIFIER
LV-CON	This paper	N/A
Chemicals, peptides, and recombinant proteins		
Recombinant Mouse DPPIV/CD26 Protein, CF	R&D Systems	954-SE; GenPept: P28843
DPP4 S624A	Sangon Biotech	NA
DPP4 Δ405-425	Sangon Biotech	NA
PD98059	MCE	HY-12028; CAS: 167,869-21-8
B-27 (50×)	Invitrogen	Cat#17504044
MG132	MCE	HY-13259; CAS: 133,407-82-6
Lactacystin	MCE	HY-16594; CAS: 133,343-34-7
Cycloheximide	MCE	HY-12320; CAS: 66-81-9
TRLZOl™ Reagent	invitrogen	Cat#15596026
MonAmpTM SYBR Green qPCR Mix	Monad	Cat#MQ10301S
Poly-L-lysine	Sigma-Aldrich	P4707; CAS: 25,988-63-0
Neurobasal medium	Invitrogen	Cat#21103049
Sitagliptin	MCE	HY-13749; CAS: 486,460-32-6
Trypsin Digestion solutions,0.25% (without phenol red)	Solarbio	Cat#T1350
SPI Chem SPI-PonTM 812 Kit	SPI-CHEM™	Cat#GS02660
2.5% Glutaraldehyde	Solarbio	Cat#P1126
Osmium tetroxide	Beijing Zhongjingkeyi Technology Co., Ltd	Cat#GP18456
Uranyl acetate	Beijing Zhongjingkeyi Technology Co., Ltd	Cat#GZ02625
Lead citrate	Beijing Zhongjingkeyi Technology Co., Ltd	Cat#GZ02618
4% Paraformaldehyde	Solarbio	Cat#P1110
Quick Antigen Retrieval Solution for Frozen Sections	beyotime	Cat#P0090
QuickBlock™ Primary Antibody Dilution Buffer for Immunol Staining	beyotime	Cat#P0262
QuickBlock™ Secondary Antibody Dilution Buffer for Immunofluorescence	beyotime	Cat#P0265
QuickBlock™ Blocking Buffer for Immunol Staining	beyotime	Cat#P0260
DAPI solution	Solarbio	Cat#C0060
QuickBlock™ Blocking Buffer for Western Blot	beyotime	Cat#P0252
QuickBlock™ Secondary Antibody Dilution Buffer for Western Blot	beyotime	Cat#P0258
QuickBlock™ Primary Antibody Dilution Buffer for Western Blot	beyotime	Cat#P0256
Rhod-2	mao kang	Cat#MX4507
lipofectamine 2000	Thermo Fisher Scientific	Cat#11668027
HitransG P	Gennechem	Cat#REVG005
Critical commercial assays		
Reactive Oxygen Species Assay Kit	beyotime	Cat#S0033S
Fastking RT Kit (with gDNA)	TIANGEN	Cat#KR116-02

(*Continued on next page*)

Continued

REAGENT or RESOURCE	SOURCE	IDENTIFIER
ATP Assay Kit	beyotime	Cat#S0026
Tissue Mitochondria Isolation Kit	beyotime	Cat#C3606
Pierce Crosslink IP Kit	Thermo Fisher Scientific	Cat#26147
Annexin V-FITC Apoptosis Detection Kit	beyotime	Cat#C1062S
MPTP Assay Kit	beyotime	Cat#C2009S
Dual Luciferase Reporter Gene Assay Kit	beyotime	Cat#RG027
ChIP Assay Kit	beyotime	Cat#P2078
Mitochondrial membrane potential assay kit with JC-1	beyotime	Cat#C2006
One Step TUNEL Apoptosis Assay Kit	beyotime	Cat#C1089
BCA Protein Assay Kit	beyotime	Cat#P0011
DPP4 Activity Fluorometric Assay Kit	BioVision	Cat#K779-100
Experimental models: Cell lines		
Primary murine hippocampal neurons	This Paper	N/A
293T(HEK293T)	ATCC	N/A
Experimental models: Organisms/strains		
Mouse: BKS.Cg-Dock7^{m} +/+ Lepr^{db}/J	Jackson Laboratory	JAX: 000,642; RRID:IMSR_JAX:000,642
Mouse: C57BL/6N-Dpp4$^{S624A/+}$	This Paper	N/A
Mouse: C57BL/6N-Dpp4^{em1cyagen}	Cyagen	Cat#KOCMP-22298-Dpp4
Oligonucleotides		
siRNA F2rl1 sense:5′-GGGCUAUCCGACUCAUCAUTT-3′ antisense:5′-AUGAUGAGUCGGAUAGCCCTT-3′	This paper	N/A
siRNA CEBPB sense:5′-GAAGUGGCCAACUUCUACUTT-3′ antisense:5′-AGUAGAAGUUGGCCACUUCTT-3′	This paper	N/A
siRNA ERp29 sense:5′-GGAGAGAAGCAAGAUGAGUTT-3′ antisense:5′-ACUCAUCUUGCUUCUCUCCTT-3′	This paper	N/A
mt-RNR2 qPCR F:5′-TGGGGTGACCTCGGAGAATA-3′ R:5′-GGATGTCCTGATCCAACATCG-3′	This paper	N/A
mt-ND6 qPCR F:5′-ACTCACTATTCGGAGCTTTACG-3′ R:5′-CAGGCTGGCAGAAGTAATCA-3′	This paper	N/A
mt-CYTB qPCR F:5′-CTAATCCACTAAACACCCCACC-3′ R:5′-GGCTTCGTTGCTTTGAGGTAT-3′	This paper	N/A
mt-COI qPCR F:5′-TCAGGAATACCACGACGCTAC-3′ R:5′-GAGGGCAGCCATGAAGTCAT-3′	This paper	N/A
IL-1β qPCR F: 5′-GAGCACCTTCTTTTCCTTCATCTT-3′ R: 5′-TCACACACCAGCAGGTTATCATC-3′	This paper	N/A
IL-6 qPCR F: 5′-CTCCCAACAGACCTGTCTATAC-3′ R: 5′-CCATTGCACAACTCTTTTCTCA-3′	This paper	N/A

(*Continued on next page*)

Continued

REAGENT or RESOURCE	SOURCE	IDENTIFIER
TNF-α qPCR F: 5′-ATGTCTCAGCCTCTTCTCATTC-3′ R: 5′-GCTTGTCACTCGAATTTTGAGA-3′	This paper	N/A
Recombinant DNA		
Plasmid: ERp29	Youbao Biological Co., Ltd	N/A
Plasmid: CEBPB	Youbao Biological Co., Ltd	N/A
Plasmid: JUND	Youbao Biological Co., Ltd	N/A
Plasmid: SP1	Youbao Biological Co., Ltd	N/A
Plasmid: pGL3	Youbao Biological Co., Ltd	N/A
Plasmid: pcDNA3.1	Youbao Biological Co., Ltd	N/A
Software and algorithms		
GraphPad Prism 9.0	GraphPad	https://www.graphpad.com/scientific-software/prism/
GEPIA	GEPIA	http://gepia.cancer-pku.cn/detail.php?clicktag=correlation###
IBM SPSS Statistics 24	IBM	https://www.ibm.com/support/pages/downloading-ibm-spss-statistics-24
JASPAR	JASPAR	https://jaspar.genereg.net/
PROMO	ALGGEN	http://alggen.lsi.upc.es/cgi-bin/promo_v3/promo/promoinit.cgi?dirDB=TF_8.3
FlowJo v10	FlowJo	https://www.flowjo.com/
KOBAS 3.0	KOBAS	http://kobas.cbi.pku.edu.cn/kobas3
STRING	STRING	https://string-db.org/

RESOURCE AVAILABILITY

Lead contact

Further information and requests for resources and reagents should be directed to and will be fulfilled by the lead contact, Tianpeng Zheng (w19831120@126.com).

Materials availability

This study did not generate new unique reagents.

Data and code availability

Data reported in this paper will be shared by the lead contact upon request. This paper does not report original code. Any additional information required to reanalyze the data reported in this paper is available from the lead contact upon request.

EXPERIMENTAL MODEL AND SUBJECT DETAILS

Ethical approval

All animal procedures were approved by the Animal Care and Experimentation Committee at Guilin Medical University and performed in accordance with approved guidelines.

Mice

Heterozygous $Lepr^{db/m}$ (db/m) mice were purchased from the Jackson Laboratory. $DPP4^{+/-}$ mice (C57BL/6N-$Dpp4^{em1cyagen}$) and $DPP4^{S624A/+}$ mice were obtained from Cyagen Bio-sciences. $DPP4^{+/-}$ mice and db/m mice were crossed to generate $DPP4^{+/-}$ db/m mice, and DPP4 KO db/db mice were generated by further breeding between $DPP4^{+/-}$ db/m heterozygous mice. $DPP4^{S624A/+}$ db/m mice were obtained by breeding $DPP4^{S624A/+}$ mice with db/m mice, and $DPP4^{S624A/S624A}$ db/db ($DPP4_m$ db/db) mice

were produced by further breeding between DPP4 $^{S624A/+}$ db/m mice. All mice used in this study were 5-month old males.

Cell isolation and culture

Hippocampus were dissected from E18 mouse embryos and dissociated with trypsin, and the neurons were plated onto poly-l-lysine-coated six-well plates and maintained in Neurobasal A medium containing 2% B27 supplement and 1% penicillin/streptomycin at 37 °C in a humidified atmosphere containing 5% CO2.

METHOD DETAILS

Stereotaxic injection

Stereotaxic injections of virus were performed in the hippocampus of adult db/m mice, db/db mice or DPP4m db/db mice. Briefly, virus were bilaterally injected in the CA1 hippocampal region at the following coordinates:x=1.0mm right or left of midline, y = −1.9mm posterior to bregma, z = 2.0mm down from surface of brain. After injection at a rate of 0.05 μl per min, the needle was left in place for 5 min before removal to prevent any leakage of the injected material. Experiments were performed 2 weeks after virus injection.

Gene silencing and overexpression

For the siRNA-mediated knockdown assay *in vitro*, primary hippocampal neurons were transfected with the ERp29 siRNA, CEBPB siRNA and PAR2 siRNA using Lipofectamine 2000, and scrambled siRNA was used as a control. Neurons were incubated 72 h prior to confirming knockdown efficiency via Western Blot. To overexpress IP3R2, ERp29 and CEBPB, primary hippocampal neurons were transfected with LV-IP3R2 (lentivirus vector expressing IP3R2), LV-ERp29 (lentivirus vector expressing ERp29), LV-CEBPB (lentivirus vector expressing CEBPB) or LV-NC (lentivirus vector expressing negative control) according to the recommended protocol. Neurons were then cultured for another 72 h and overexpression efficiency was verified by immunoblot analysis.

To knockdown IP3R2, ERp29, CEBPB, and PAR2 *in vivo*, specific short-hairpin RNA (shRNA) sequence was cloned into adeno-associated virus (AAV) vector. IP3R2 AAV, ERp29 AAV, CEBPB AAV, PAR2 AAV or AAV control virus was injected into the hippocampus. For IP3R2, ERp29 and CEBPB overexpression, IP3R2, ERp29 and CEBPB overexpression adeno-associated virus (AAV-IP3R2, AAV-ERp29 and AAV-CEBPB) were used to overexpress IP3R2, ERp29 and CEBPB in the hippocampus. After the treatment, samples were harvested and used for subsequent experiments, knockdown and overexpression efficiency was verified by immunoblot analysis.

Isolation of MAM

MAM was isolated from hippocampus following an established protocol as previously reported.[23] Briefly, hippocampus isolated from mice was homogenized on ice. Then, the homogenate was centrifuged at 1000 × g for 5 min to obtain the supernatant. Collected supernatant was centrifuged at 3500 × g for 10 min to separate crude mitochondria. The crude mitochondrial fraction was re-suspended in 2 ml mitochondrial re-suspension buffer (250 mM mannitol, 5 mM HEPES, pH 7.4, and 0.5 mM EGTA), layered on top of 30% percoll medium (225 mM mannitol, 25 mM HEPES, pH 7.4, 1 mM EGTA), and centrifuged at 95,000× g for 30 min. The crude MAM fraction was isolated from percoll gradient and further purified by centrifugation.

Immunoprecipitation and immunoblot analysis

The hippocampus and primary hippocampal neurons were homogenized in a solution containing 1% proteinase inhibitor (MCE) and phosphatase inhibitors (MCE). Samples were centrifuged at 12,000×g for 10 min and the supernatant were subjected to immunoblot analysis or immunoprecipitation. For immunoprecipitation, the lysates were incubated with specific antibodies together with Protein A/G Plus Agarose (Thermo Scientific) according to the manufacturer's manual. The immunoprecipitates were collected and boiled in SDS loading buffer. For western blot, protein samples were subjected to SDS–PAGE and transferred to PVDF membranes. Subsequently, membranes were blocked in QuickBlock™ Blocking Buffer (Beyotime), incubated with specific primary antibody overnight at 4 °C, and followed by incubation with horseradish peroxidase-conjugated secondary antibodies at room temperature for 1 h. All antibodies were summarized in the key resources table. Immunoreactive signals were detected by chemiluminescent ECL Substrate kit (Bridgen) and quantified by Image Lab.

For co-IP analysis, 293T cells were cotransfected with vectors expressing Flag-IP3R2 and either HA-ERp29, HA-ERp29 (b-type PDI domain), or HA-ERp29 (D-domain). 293T cells or primary hippocampal neurons were homogenized in CoIP buffer. Cell lysates were incubated overnight with an anti-Flag, anti-ERp29 or anti-IP3R2 antibody, and coupled with protein A/G agarose beads. Immunoprecipitated complexes were collected and subjected to immunoblot analysis using the indicated antibodies.

RNA extraction and RT-qPCR

Total RNA was extracted from primary hippocampal neurons and hippocampus by standard procedure using Trizol Invitrogen. cDNA was synthesized using FastKing RT Kit (TianGen). Quantitative PCR was performed using SYBR green fluorescent dye (Monad) according to manufacturer's instructions. Fold change in mRNA expression of target mRNA was normalized to GAPDH and calculated using the $2^{-\Delta\Delta CT}$ method.[5]

Immunofluorescence

Immunofluorescence staining was performed on 4% PFA fixed hippocampal cryosections. Antigen retrieval was performed using Quick antigen retrieval solution (Beyotime). After antigen retrieval, sections were blocked with QuickBlock™ Blocking Buffer (Beyotime) for 1 h, incubated with respective primary antibodies overnight at 4 °C, and followed by incubation with secondary antibodies at room temperature for 1 h (protected from light). Subsequently, DAPI (5 ug/ml) was used to counterstain sections and images were acquired with a fluorescence microscope (Olympus).

Chromatin immunoprecipitation

The Chromatin immunoprecipitation (ChIP) assay was performed with ChIP Assay Kit (Beyotime). Briefly, primary hippocampal neurons were cross-linked in 1% formaldehyde. The cross-linking reaction was stopped by Glycine Solution. Primary hippocampal neurons were lysed in SDS buffer containing PMSF and lysates were sonicated into fragments with a mean length of 200–1000 bp at 4 °C. The DNA–protein complexes were subjected to immunoprecipitation with IgG and CEBPB antibodies. After washing with salt buffers, the precipitated DNA fragments were eluted and purified with the PCR Clean Up Kit and then quantified by RT-qPCR.

Mitochondrial membrane potential assay

The mitochondrial membrane potential was measured by using JC-1 Mitochondrial Membrane Potential Assay Kit (Beyotime). Briefly, primary hippocampal neurons and mitochondrial fractions isolated from hippocampus were stained with JC-1 for 20 min. JC-1 monomers and aggregates were detected as green and red fluorescence respectively, with mitochondrial membrane potential depolarization revealed as a decrease in red: green fluorescence intensity.

ATP measurement

ATP levels in primary hippocampal neurons and hippocampus were determined using the ATP assay kit (Beyotime). Briefly, the supernatant was suspended in standard reaction buffer containing luciferin and luciferase following the manufacturer's instructions, and luminescence read at a multifunctional microplate reader.

Detection of reactive oxygen species (ROS)

ROS production in primary hippocampal neurons and mitochondrial fractions isolated from hippocampus was analyzed by flow cytometry using fluorogenic probe MitoSOX (Thermo Scientific) or DCFH-DA (Beyotime) according to the manufacturer's protocol.

Apoptosis analysis

Apoptosis in primary hippocampal neurons was assayed using Annexin V-FITC Apoptosis Detection Kit (Beyotime). Primary hippocampal neurons were incubated with annexin V-FITC and Propidium iodide according to the manufacturer's instructions. Data acquisition was performed on a URIT flow cytometer and analyzed with FlowJo v10 (Ashland).

Mitochondrial Ca^{2+} measurement

To measure mitochondrial Ca^{2+} levels, primary hippocampal neurons were incubated with Rhod-2 probe and Pluronic F-127 for 30 min at 37 °C. Rhod-2 signal were calculated by flow cytometry (URIT). The collected data were analyzed with FlowJo v10.

Transmission electron microscopy (TEM)

To view ER and mitochondria contact, hippocampus isolated from mice and primary hippocampal neurons were fixed with 2.5% glutaraldehyde overnight and post-fixed with 1% osmium tetroxide for 2 h. After dehydration in a graded series of ethanol and acetone, samples were embedded in Epon 812 resin and sliced with an ultramicrotome. The ultrathin sections were poststained with uranyl acetate and lead citrat, and viewed using a Hitachi-HT7700 electron microscopy (Hitachi). The ER mitochondrial contacts were quantified. The mitochondria and ER physically interact to form domains defined as mitochondria-associated ER membranes (MAMs), where the outer mitochondrial membrane is close to the ER (within 10–30 nm).[46] On the images, we drew a line with the Image J software, marking and measuring the shortest distance between the outer mitochondrial membrane and the nearest ER membrane.

TUNEL staining

Tissue sections were stained with TUNEL according to TUNEL Apoptosis Assay Kit (Beyotime, C1088). Briefly, sections were treated with 0.1 % Triton X-100 for 5 min and incubated with TdT enzyme solution for 1 h at 37 °C. After washing in PBS, the nuclei were then counterstained with DAPI (5 μg/ml) for 10 min at room temperature. Images were obtained using a fluorescence microscope.

MPTP

MPTP in primary hippocampal neurons was assessed using the calcein/CoCl2 method. Primary hippocampal neurons were stained with calcein AM in the presence or absence of CoCl2 for 30 min at 37°C. Calcein signal was monitored by fluorescence microscope.

Luciferase assays

Luciferase activities in cultured 293T cells were assayed with the Dual Luciferase Reporter Gene Assay Kit following the manufacturer's protocol. 293T cells were co-transfected with corresponding plasmids. The relative firefly luciferase activity was normalized to Renilla luciferase activity to compensate for variability in transfection efficiencies.

Morris water maze

Each mouse was given 4 trials a day for five consecutive days. The searching time taken to locate the platform was calculated. At the end of training on the fifth day, Mice were given a probe trial in which the platform was removed from the pool. All behavioral parameters (platform crossings, time in target quadrant, and the swimming paths) were recorded using Video Tracker software (Anymaze).

Active avoidance memory test

To assess auditory learning and memory of mice, the active avoidance test was conducted using a shuttle BOX (Xinruan, Shanghai, China). During the training session, each mouse was given two trials a day for three consecutive days. The avoidance responses of the mice were calculated and analyzed.

DPP4 enzyme activity

DPP4 enzyme activity in hippocampus obtained from mice was measured using the DPP4 Activity Fluorometric Assay Kit (BioVision, Cat#K779-100). DPP4 enzyme activity in tissue was normalized to total protein content.

Bioinformatics analysis

Publicly available proteomic data for the MAM of db/db mice was used for bioinformatics analysis.[23] Heatmaps showing differential expression analysis (DEGs) were generated using Microsoft Excel. Volcano plots for visualization of DEGS were plotted using GraphPad. Functional enrichment analysis of DEGs were performed using the KOBAS 3.0 website (http://kobas.cbi.pku.edu.cn/kobas3). Protein-interaction network analysis was performed to identify signaling using the STRING database (https://string-db.org/).

QUANTIFICATION AND STATISTICAL ANALYSIS

Statistical analysis and data graphics were analyzed and plotted with GraphPad Prism 9.0 software (GraphPad Software). Statistical significance was assessed using unpaired two-tailed Student's t tests when the experiment contained two groups, or ANOVA when comparing more than two groups. All numerical data were expressed as mean ± standard error of the mean (SEM). Values of p below 0.05 were regarded as statistically significant. In figures, asterisks represent statistical significance (*p <.05, **p <.01, ***p <.001)